MeerKAT L Band Beam Correction

W. D. Cotton (NRAO), M. de Villiers (SARAO), K. McAlpine (SARAO) November 23, 2025

***Abstract*—This memo examines MeerKAT L band observations of a series of offset pointings of a strong polarized calibrator and a strong unpolarized calibrator using reference pointing. There were 8 offset positions on a ring 0.83° around the source position which were observed cyclically. Observations were sufficiently extended in time that beam rotation due to parallactic angle caused the traces of the location in the beam sampled to overlap. Observations were made in March and July 2025. In the July sessions a single MeerKAT extension antenna, e121, was included. The observations were compared with the values expected from beam effects derived from antenna averaged holography beam models. The comparison is good if not perfect. Imaging applying beam corrections shows good results. Improved consistency in derived source brightness is notable, especially in the linearly polarized Stokes parameters Q and U.**

***Index Terms*—Antenna pattern corrections**

I. Introduction

ONE of the tests of understanding antenna beam patterns is to make measurements of a bright source at a number of locations offset from the center of the beam and determine if the beam model can reproduce the observations using only the Stokes I,Q,U and V of the source. To reduce the pointing uncertainty, reference pointing is desirable.

The simplest test is to verify that a simple model of the source combined with measured beam patterns can reproduce the observations. The ultimate test is to image these data applying corrections from the measured beam patterns resulting in lowered artifacts and more nearly correct images. The technique used in the following to apply these corrections during imaging is that described by [1].

The general approach is to make dirty/residuals images using no corrections but doing a proper inclusion of the effects of the antenna patterns when calculating the interferometer response to the sky model which is subtracted from the visibilities. In order to avoid amplifying image noise, the sky model subtracted from the visibilities is appropriate for the antenna type with the narrowest (widest?) primary beam. The resultant image will thus have an effective primary beam of an antenna of the largest (smallest) of the antennas diameter used, with a circularly symmetric beam. After multiple major cycles, the accumulated sky model converges towards the correct value and the residual images towards noise.

This memo describes a number of tests using reference pointed offsets from a bright unpolarized source (J0408-6545) and a bright polarized source (3C138=J0521+1638). Several of the tests also included a single MeerKAT extension antenna, e121. Data were analyzed in the Obit [2][1] system.

National Radio Astronomy Observatory, 520 Edgemont Rd., Charlottesville, VA, 22903 USA email: bcotton@nrao.edu

[1]http://www.cv.nrao.edu/∼bcotton/Obit.html

TABLE I
Offset Pointing Tests

Date	CBID	Source	Length hrs.
03 Mar 2025	1741018428	3C138	3.5
23 Jul 2025	1753257570	J0408-6545	5.5
25 Jul 2025	1753422205	3C138	4.5

II. Offset Pointing Tests

A. Observations

The tests consisted of cyclic observations of eight offsets of each source in a circle of radius 0.83° around the source position. Each test was long enough that the rotation of the antenna pattern on the sky due to parallactic angle caused the locus of sampling of the beam from one of the offsets to overlap with that of another. The dates and lengths of the tests are given in Table I and the positions of the calibrators and offset positions are in Tables II and III.

Data were in L Band (856–1712 MHz) with 4K spectral channels and all four combinations of the linear feeds recorded. Data for these tests were divided into 8 spectral windows (IFs) each with either 119 channels of 0.836 MHz width (March 2025) or 238 channels of width 0.418 MHz (July 2025). The March 2025 data used 8 second dumps and the July 2025 data, 4 second. Offset pointing measurements were made on the target source every 20 min, followed by an on–axis gain calibration scan and a cycle among the offset positions with 2 min. on each. J0408-6545 was used as the flux density/delay/bandpass/unpolarized calibrator and 3C138 was the polarized calibrator. The March 2025 data were calibrated in Tom Mauch's Obit based calibration pipeline with subsequent polarization calibration in Obit. The July 2025 data were calibrated in the revision of the older pipeline which also includes an improved polarization calibration [3]. The July data included a single MeerKAT extension antenna, e121, which was calibrated with the MeerKAT antennas.

B. Comparison with beam models

In order to compare the observations with the beam models, the data were shifted to the position of the source, averaged over baseline in 30 second intervals and 0.416 or 0.835 MHz channels (∼2000 or ∼1000 channels). For data including the MeerKAT Extension antenna, separate files were made including only MeerKAT baselines and all MeerKAT-MeerKAT Extension antenna baselines. A comparison of the data with

TABLE II
OFFSET POINTINGS OF 3C138

Name	RA (2000)	Dec (2000)
J0521+1638	05 21 09.89	16 38 22.1
J0521+1728	05 21 09.89	17 28 22.1
J0524+1714	05 23 37.95	17 13 40.1
J0525+1638	05 24 38.63	16 38 15.5
J0524+1603	05 23 37.04	16 02 57.5
J0521+1548	05 21 09.89	15 48 22.1
J0519+1603	05 18 42.73	16 02 57.5
J0518+1638	05 17 41.15	16 38 15.5
J0519+1714	05 18 41.82	17 13 40.1

TABLE III
OFFSET POINTINGS OF J0408-6545

Name	RA (2000)	Dec (2000)
J0408-6545	04 08 20.38	-65 45 09.1
J0408-6455	04 08 20.38	-64 55 09.0
J0414-6509	04 13 57.02	-65 09 24.0
J0416-6544	04 16 27.22	-65 44 20.7
J0414-6620	04 14 12.75	-66 20 05.7
J0408-6635	04 08 20.38	-66 35 09.2
J0402-6620	04 02 28.01	-66 20 05.7
J0400-6544	04 00 13.53	-65 44 20.7
J0402-6509	04 02 43.74	-65 09 24.0

model values derived from the average antenna beams for each MeerKAT and MeerKAT Extension was made by plotting the values as a function of orientation in the antenna pattern (from north thru east). All offset measurements used an offset of 0.83°. The source in question was imaged in Stokes I,Q,U and V to derive its spectrum. For each comparison, the integrated Stokes I,Q,U and V (assumed 0) were used with the beam images interpolated to the position in the beam in which the source was being observed to predict the visibility. The details are outlined in the following sections.

1) Beam location: For each offset position, the offset in RA (dRA) and declination ($dDec$) as projection cosines from the true source position were determined. The orientation in the beam (PA_Offset) at transit is

$$PA\_Offset \ = \ \mathrm{atan2}(dRA, dDec).$$

If χ is the parallactic angle of the source then the beam angle of the datum as plotted is

$$BA \ = -PA\_Offset \ + \chi.$$

The corresponding point in the beam is at offset dRA, $dDec$ rotated by -χ.

2) Model Vis. from beam: A python routine to compute the model visibility is given in Figure 1.

C. Results

The comparison for a single channel towards the top of L Band are given in Figure 2 for March 2025, Figures 3 and 4 show the observation of the polarized source 3C138 on 25 Jul 2025 for the MeerKAT only and MeerKAT-MeerKAT Extension baselines. Figures 5 and 6 give the comparison for the unpolarized source J0408-65 on 23 July 2023 for the MeerKAT only and MeerKAT-MeerKAT Extension baselines.

III. ISSUES

- The dipoles in e121 are rotated by 180 degrees from those in MeerKAT antennas. How this affects the polarization calibration is unclear. No attempt was made to correct for this. Was some of this absorbed into the parallel hand phase calibration?
- The XX and YY, esp. the imaginary parts of the MeerKAT-MeerKAT Extension data do not show good agreement between data and model. This is in contrast with XY and YX. This may be due, in part, to the parallel hand data calibration absorbing phase contributions due to the difference in antenna beams.

IV. IMAGING J0408-6545 OFFSETS WITH MFBEAM

Obit program MFBeam is a wide–band, wide–field imager similar to MFImage [4] which makes corrections based on images of the antenna patterns. It can currently make corrections for arrays containing two antenna designs such as MeerKAT and MeerKAT Extension antennas. Beam images as 1024 channel cubes across L Band are available.

The test data being analyzed in this memo presents some challenges for the CLEAN software. The data consists of observations of very bright sources on the shoulders of the antenna power pattern which imposes strong curvature in the apparent spectrum of the source. CLEAN, as practiced in Obit MFImage and MFBeam, involves iteratively decomposing a set of subband images into "components" and then Fourier transforming and subtracting this relatively broadband model from each spectral channel. The scheme currently used in MFImage is to fit a power law spectrum to the subband flux densities in each component and using the spectral index to extrapolate the nearest subband flux density to a given frequency channel. A spectral index of zero (flat spectrum) is used if the fitting fails. This works well near the beam center where the apparent spectra of most sources is close to power law. However, for bright sources on the shoulder of the beam, the variable gain across the wide MeerKAT bandpass introduces strong curvature to the apparent spectrum and this scheme is sub-optimal. The estimation of the antenna pattern effects being modeled by MFBeam depends critically on knowing accurate flux densities in each channel.

A further complication is that the spectral fitting imposes some sanity checks and disregards fits producing spectral indices with physically impossible values, e.g. -6, which are possible for sources on the shoulders of the beam but not are representative of the whole spectrum.

```
def CalcModVis(Stok, gxx, gxy, gyx, gyy, hxx, hxy, hyx, hyy, PA, I, Q, U, V):
    """
    Return model visibility for Stokes Stok

    Stok                  Stokes correlation of vis e.g. "XX", "YY", "XY", "YX"
    gxx, gxy, gyx, gyy,   complex gains of the 1st antenna
    hxx, hxy, hyx, hyy,   conjugate of gains of 2nd antenna
    PA                    Parallactic angle (deg)
    I,Q,U,V               Stokes parameters
    return complex visibity
    """
    c2p = cos(rad(2*PA)); s2p = sin(rad(2*PA))
    J = complex(0.,1.)
    # Product for this Stok
    if Stok=='XX':
        gc = I*(gxx*hxx + gyx*hyx) + \
             Q*(c2p*(gxx*hxx-gxy*hxy)-s2p*(gxy*hxx+gxx*hxy)) + \
             U*(c2p*(gxy*hxx+gxx*hxy)+s2p*(gxx*hxx-gxy*hxy)) + \
             J*V*((gxx*hxy-gxy*hxx))
    elif Stok=="YY":
        gc = I*(gxy*hxy + gyy*hyy) + \
             Q*(c2p*(gyx*hyx-gyy*hyy)-s2p*(gyy*hyx+gyx*hyy)) + \
             U*(c2p*(gyy*hyx+gyx*hyy)+s2p*(gyx*hyx-gyy*hyy)) + \
             J*V*(gyx*hyy-gyy*hyx)
    elif Stok=="XY":
        gc = I*(gxx*hyx + gxy*hyy) + \
             Q*(c2p*(gxx*hyx-gxy*hyy)-s2p*(gxy*hyx+gxx*hyy)) + \
             U*(c2p*(gxy*hyx+gxx*hyy)+s2p*(gxx*hyx-gxy*hyy)) + \
             J*V*(gxx*hyy-gxy*hyx)
    elif Stok=="YX":
        gc = I*(gyx*hxx + gyy*hxy) + \
             Q*(c2p*(gyx*hxx-gyy*hxy)-s2p*(gyy*hxx+gyx*hxy)) + \
             U*(c2p*(gyy*hxx+gyx*hxy)+s2p*(gyx*hxx-gyy*hxy)) + \
             J*V*(gyx*hxy-gyy*hxx)
    return gc
```

Fig. 1. Python routine to compute model visibilities from beam gains, Stokes parameters and the parallactic angle.

The estimation of channel flux densities from the subband flux densities in MFBeam now uses the following scheme.

1) **Effective subband frequency.** Due to RFI flagging, the effective frequency of a given subband may not be the band center. The effective subband frequencies are estimated from the data weights after applying flagging, calibration and Robust weighting. These values are stored to the image headers and used in evaluating spectra.
2) **Spectral Fit** to the subband flux densities in each component. This uses a 4 term curved power law fit to follow the effects of frequency variable antenna gain as well as non power law source spectra. The fitting uses measured robust RMSes in each subband image. This is only done for Stokes I components, for polarized components a flat spectrum is assumed.
3) **Weak/negative components** CLEAN must allow negative components to correct any over–subtraction. Such components cannot be fitted by a power law. If the component spectrum is too weak to be fitted and/or contains non-positive values, a flat spectrum is assumed.
4) **Evaluate Spectrum,** the fitted (or flat) spectrum is evaluated at the channel frequency and at the effective frequency of the closest subband. The ratio of these two is used to extrapolate the subband flux density to the channel frequency.

To simplify the initial testing, only data using MeerKAT antennas were used and the top of the band where the OMTs become problematic was dropped. Furthermore, these tests used the J0408-6545 data for which the source is very weakly polarized and all apparent polarized emission can be assumed spurious. Data for these tests consist of 8 spectral windows (IFs) each with 238 channels of 0.418 MHz width.

The artifacts and instrumental polarization to be removed are a linear function of the true Stokes I intensity; only the brighter components really need to be considered in calculating the spurious polarized response. A threshold was implemented in MFBeam. If the sum of the mid-band com-

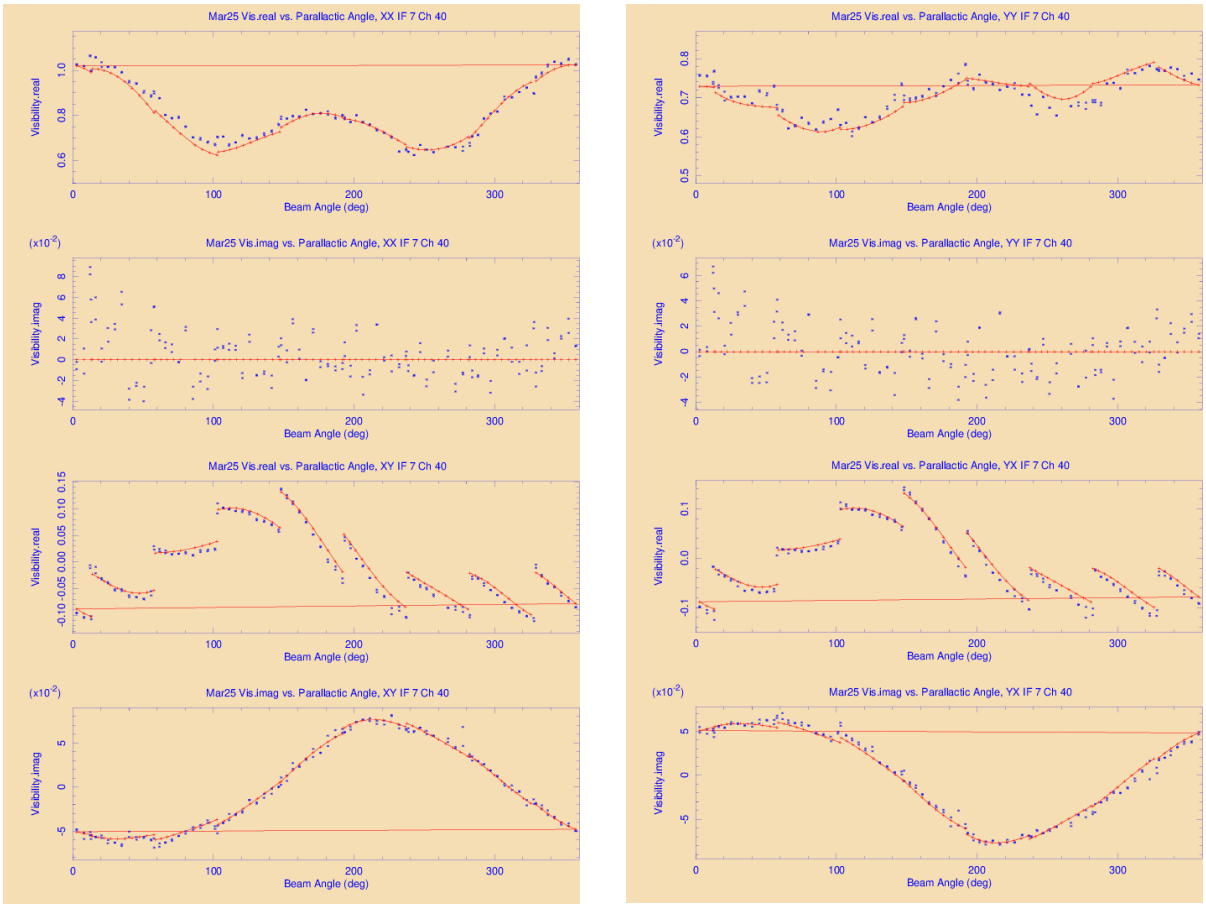

Fig. 2. 3C138 reference pointed offset data from 03 Mar 2025. Baseline and 30 second averages for channel 40 in IF 7, ν=1.6654 GHz. Upper left panel is XX, upper right is YY, lower left is XY and lower right is YX. The real part is shown in the upper plot and the imaginary part in the lower plot. Averaged data is shown in blue and the corresponding model value is shown as red points connected by a red line.

ponent flux densities in a given major cycle exceeds this value, the data are evaluated with the Jones matrices obtained from the beam images. Otherwise, unit Jones matrices (no correction) are used. This both reduces the computation time (the unit matrices don't change with frequency or parallactic angle) and allows turning off the corrections entirely. This latter feature allows a more rigorous comparison of imaging with and without the beam corrections.

A. Model and Data v. Beam Angle

Each offset pointing on the unpolarized source J0408-6545 was imaged using MFBeam using only MeerKAT baselines and a threshold of 100 mJy/beam. A single pass at phase only self calibration was used in both images. Since only MeerKAT antennas were used, the beam corrections will not affect the parallel hand phases. Task UVPolCor was used to create model data sets using the MFBeam CLEAN model applying beam corrections. Figures 7 and 8 show baseline averaged data (blue) and model (magenta) and a simple model of the source (red) as a function of beam angle for spectral channels near the bottom and near the top of the band. The magenta model points generally, but not always, follow the blue data points.

B. With and Without Beam Correction Comparison

Images with and without beam corrections were both done with MFBeam, one with a large threshold such that beam corrections were never used and one with the threshold set at 100 mJy/bm (∼5% of peak). CLEAN was restricted to a single 3 pixel radius circular box centered on the source position. Since the source is not expected to show real polarized emission, only Stokes I was effectively CLEANed. The central portions of the residual images (CLEAN components not restored) are shown in Figures 9 – 16 for data in each of the 8 offset pointings.

Applying the beam corrections result in a significantly lower level of artifacts. This is especially true of Stokes Q, U and V where all apparent emission is an artifact and when the uncorrected images have brighter artifacts.

V. Imaging of J0408-6545 offsets using MK+MKE

Further imaging tests were performed similar to those described in Section IV on the J0408-6545 offset pointings using baselines including the MeerKAT Extension antenna e121. As before, the data were phase self calibrated. Tests using beam correction used MFBeam with a threshold of 100 mJy/beam, those without corrections used a threshold of 1000 Jy/beam. All of L band was used in these tests. Comparisons

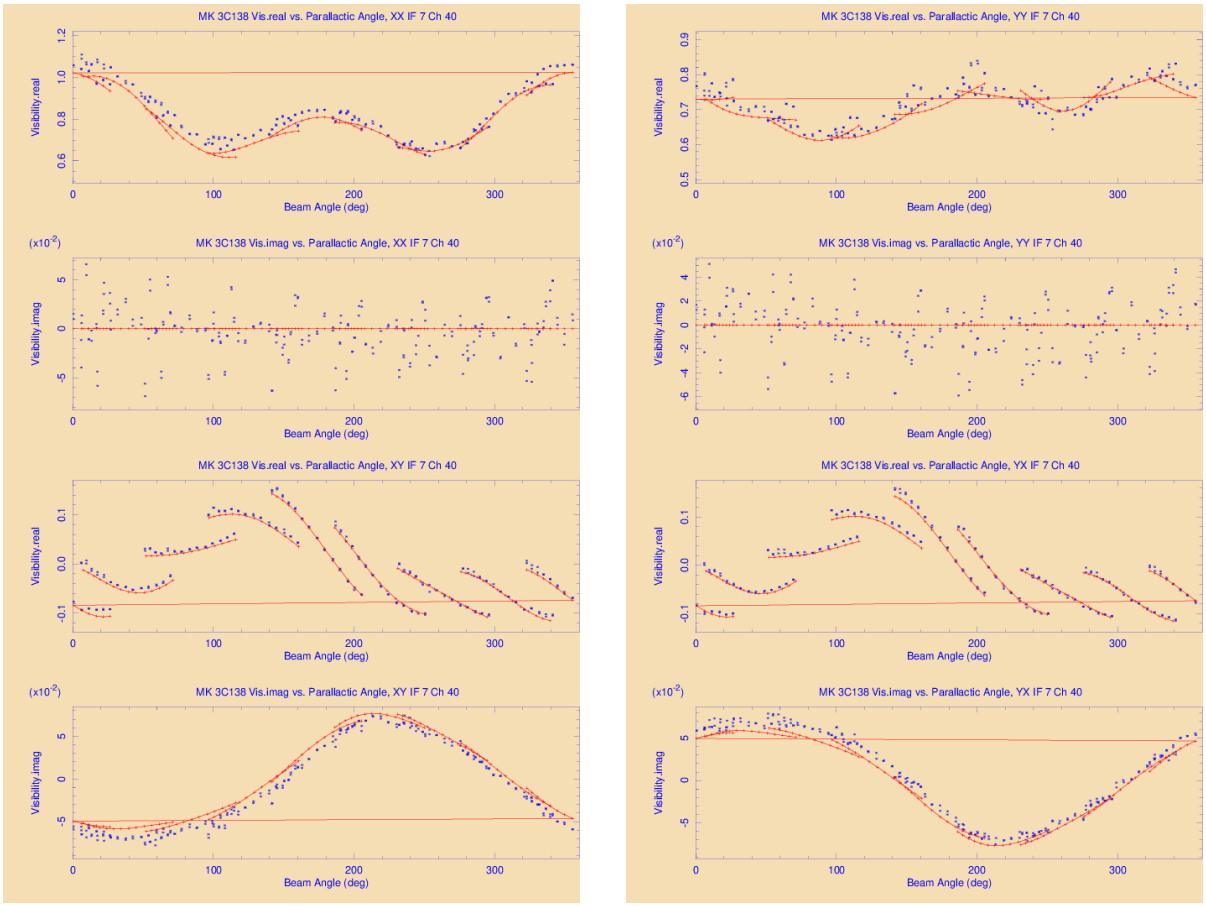

Fig. 3. Like Figure 2 but 3C138 reference pointed offset data from 25 July 2025 on baselines among MeerKAT antennas.

of the imaging with and without beam corrections are given in Figures 17 – 24. Application of the beam corrections substantially reduced the level of artifacts in the residual images. The uncorrected images including MeerKAT Extension antennas (Figs 17–24 generally have stronger artifacts than those using only MeerKAT antennas (Figs 9–16) whereas the corrected images tend to have similar qualities.

VI. X-Y Phase Calibration Revisited

One of the components of the initial polarization calibration of the data considered here, the phase difference between the two linearly polarized feed systems (AKA "X-Y phase), used Obit program XYDly [5]. This program solves for a residual X-Y phase and delay in each of the 8 spectral windows. This is apparently insufficient to fit the variations in the residual X-Y phase, especially at lower frequencies where the noise is higher and the polarized emission from calibrators weaker and can leave errors of several degrees. This is sufficient for rotate some of the linear polarization into circular.

An improved technique, XYPass, like XYDly, uses the fact that on calibrated XY and YX baselines, the real part is solely a function of linear polarization and the imaginary part, solely circular. For sources in which the circular polarization can be assumed to be zero, the X-Y phase can be derived directly from the phases of these data. Example plots are shown in Figure 25 illustrating the fine scale frequency structure in the March and July 2025 observations of 3C138. The July data is more heavily edited but the same reference antenna (m059) was used for both. These data have had X-Y phases corrections from the DelayCal before the observation applied so the instrumental contributions from the downstream electronics have been removed. The X-Y residual phase function will be dominated by that of the OMT on the reference antenna. Regions of the March spectrum appear affected by unflagged RFI whereas these have been flagged in the July data.

VII. Polarized Calibrator (3C138)

A. March 2025

The first imaging test of a polarized calibrator is that of the 03 March 2025 series of offset pointings of 3C138 (J0521+163). This data contains only MeerKAT antennas. The offset pointings were imaged with (Threshold=10 mJy/bm) and without beam corrections (Threshold=1000 Jy/bm) with a single phase self calibration.

1) Image Extrema: One measure of the effectiveness of the beam corrections is how well they recover the source flux densities. The same source is being observed in the various offsets which are all at the same angular offset but the portion of the beam being looked through will vary the apparent brightness. The extrema, generally the flux density at the

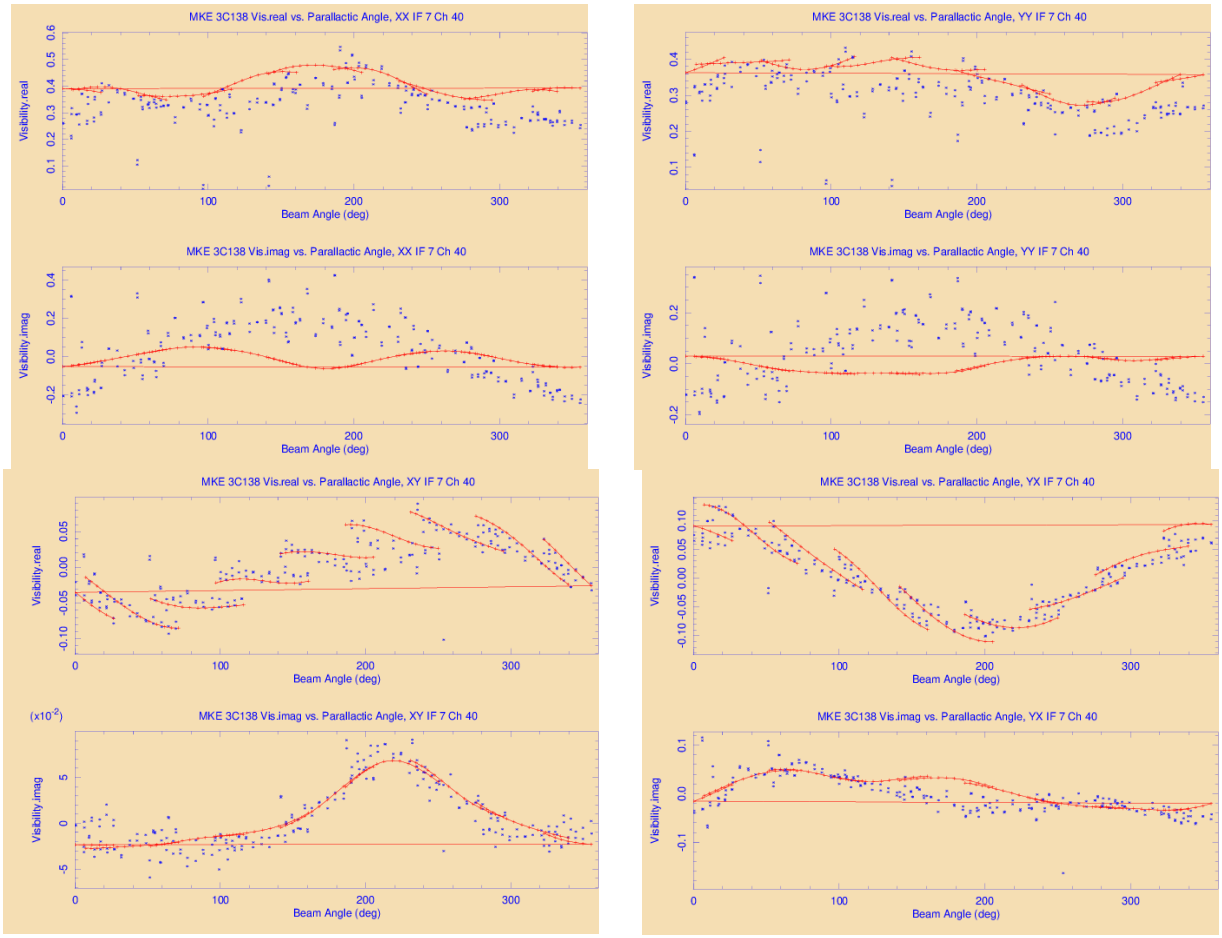

Fig. 4. Like Figure 2 but 3C138 reference pointed offset data from 25 July 2025 on baselines between MeerKAT antennas and MeerKAT Extension antenna e121.

source position, of the various offsets and Stokes parameters is given in Table IV. This table gives the values both with and without the beam corrections; the RMS of the values in each column is given in the bottom row. With the exception of Stokes V, for which no detection was expected, the scatter in the uncorrected images is one or two orders of magnitude larger than in the corrected images. The beam corrections dramatically improve the consistency of the Q and U flux densities.

2) Gain Corrected Values: The imaging process described here should result in images with pixel values that would have been obtained with an array, all of who's antennas had the symmetric beam pattern applied in the imaging. [1] suggest using a symmetric beam corresponding to the largest antenna used to avoid amplifying the image noise. In the imaging presented here, using a 15 m "perfect" beam led to instabilities in the CLEANing as it approached to noise level. This is possibly because only a very small fraction of the data involved the larger antenna size and the corrections were very large. As a result, the imaging described here used a symmetric 13.5 m beam pattern. The gain of this pattern at the reference frequency of 1.2838 GHz at the offset (0.83°) used in these tests is 0.1955. Thus, the peak values at the reference frequency in the derived images when corrected by this gain are expected to be approximately those derived from the pointing directly at the calibrator. Such an analysis is shown in Table V which compares the average gain corrected peaks with and without the beam corrections applied in imaging of the offset pointings to the center pointing.

The expected result is not seem in Table V; both the corrected and uncorrected image averages are systematically below the expected value by some 10–15%; the corrected values have a more consistent ratio.

3) Image Comparison: The comparison of imaging with and without beam corrections is given in Figures 26–33. With a few exceptions, the level of off–source artifacts is not very different with and without beam corrections.

4) Data–Model Comparison: The baseline and 30 second data and model comparisons are shown in Figures 34 and 35. The data (blue) and models (magenta) values show generally good agreement except for the real parts of IF 1, channel 92 XY and YX in which the sequence for each offset pointing has an increasing separation towards lower beam angles (later times). This is possibly an artifact of the data being averaged in time rather than parallactic angle.

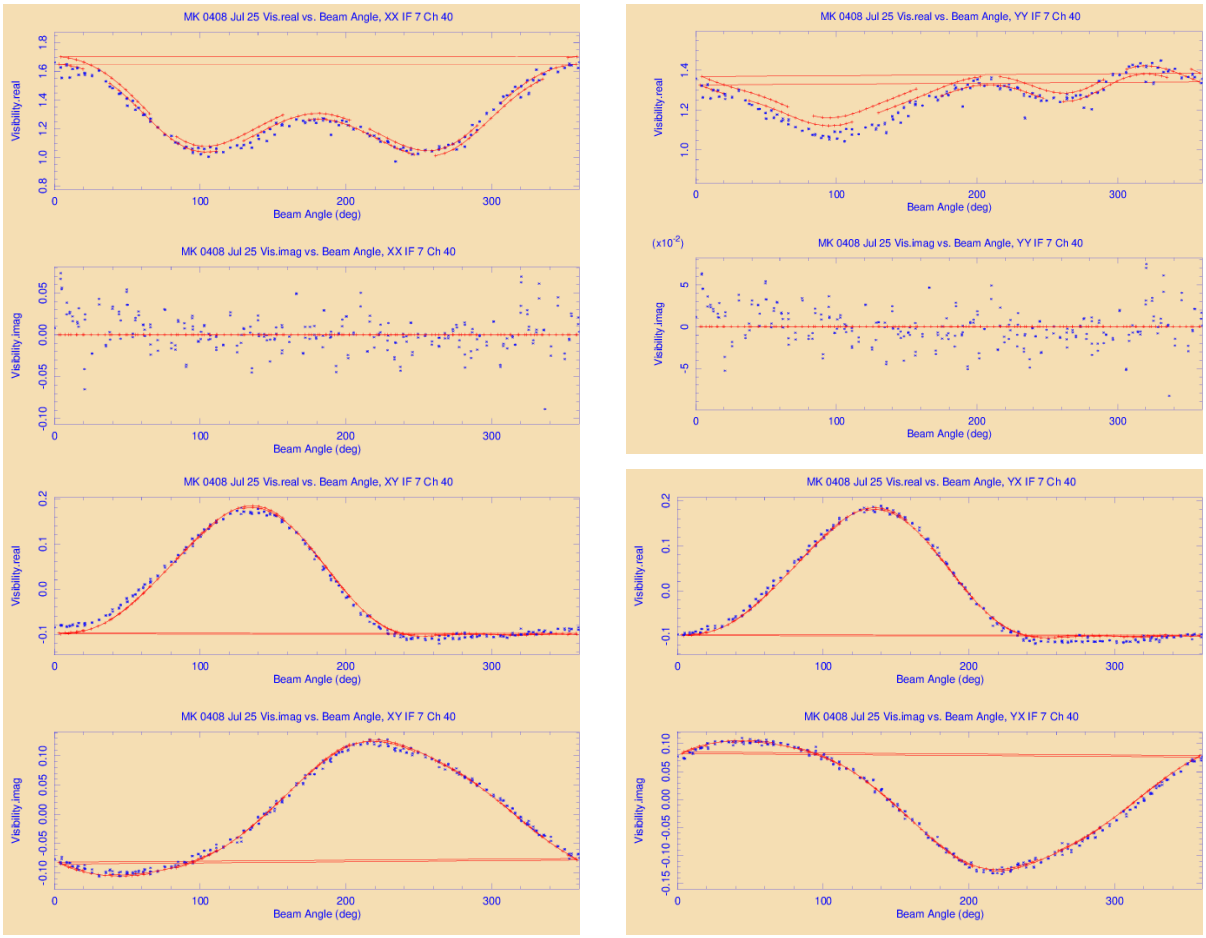

Fig. 5. Like Figure 2 but J0408-6545 reference pointed offset data from 23 July 2025 on baselines among MeerKAT antennas.

B. July 2025

The second imaging test of a polarized calibrator is that of the 25 July 2025 series of offset pointings of 3C138 (J0521+163) which included a single MeerKAT Extension antenna, e121. The offset pointings were imaged with (Threshold=10 mJy/bm) and without beam corrections (Threshold=1000 Jy/bm) with a single iteration of phase self–calibration.

1) Image Extrema: The consistencies of the extrema in the various offset pointing images with and without beam corrections was compared as was done in Section VII-A1. The extrema, generally the flux density at the source position, of the various offsets and Stokes parameters is given in Table VI. This table gives the values both with and without the beam corrections; the RMS of the values in each column is given in the bottom row. With the exception of Stokes V, for which no detection was expected, the scatter in the uncorrected images is one or two orders of magnitude larger than in the corrected images. The improvement in consistency is especially dramatic for the linearly polarized Stokes parameters Q and U.

2) Gain Corrected Values: As for the data presented in section VII-A2, the offset pointings were corrected by the gain with averages being compared to the on-axis pointing values. This comparison is given in Table VII;. As for Table V, the gain corrected values are lower than the on–axis values and by a similar amount (10-15%). The cause of this discrepancy is unclear but may be related to the very large offset used for these tests. The fact that both the corrected and uncorrected images show a similar reduction in amplitudes suggests the cause is common to both. A coherence loss due to the large offsets used is one possibility. However, imaging dropping the baselines to MeerKAT extention antenna e121 gave similar results. The longer baselines using e121 were more susceptible to time and delay smearing.

The calibration procedure used for the test presented here used a baseline dependent time averaging which should not have caused significant time smearing within a radius of 1° of the pointing center. As a final test, the July 2025, 3C138 data were recalibrated without this averaging to see if it were somehow related to the reduced amplitudes. The comparison of gain corrected peak values with and without beam corrections is shown in Table VIII. Both have similar reductions of the amplitudes and for Stokes I the reduction is even greater than with time averaging.

3) Image Comparison: The comparison of imaging with and without beam corrections is given in Figures 36–43. As opposed to the March 2025 observations which included only MeerKAT antennas, the inclusion of even a single MeerKAT

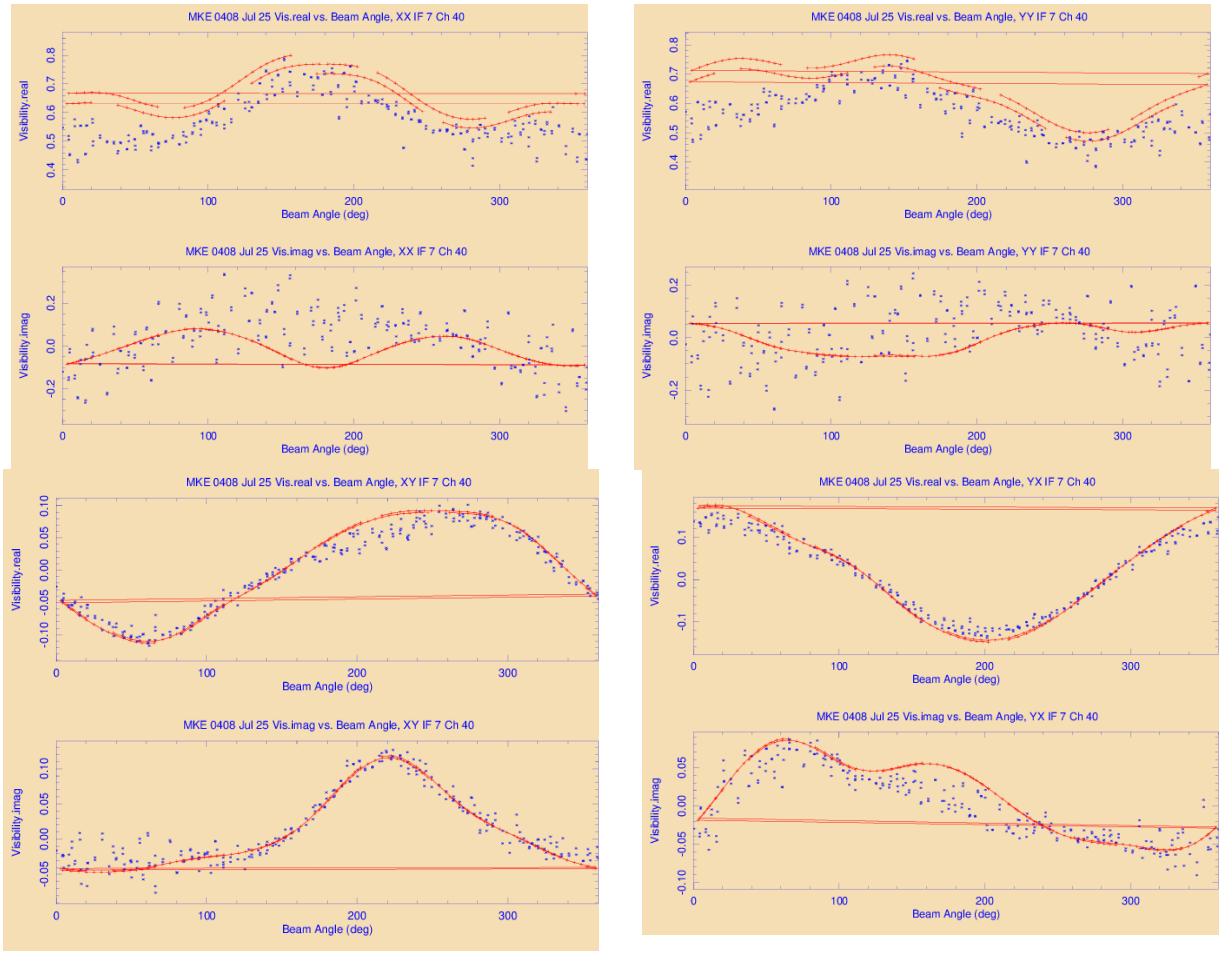

Fig. 6. Like Figure 2 but J0408-6545 reference pointed offset data from 23 July 2025 on baselines between MeerKAT antennas and MeerKAT Extension antenna e121.

Extension antenna significantly increases the level of visible artifacts in most of the offset pointings. This is due to the difference in the beam patterns of the two antenna designs at the radius they are being sampled in this data set. The beam corrections remove the worst of these.

4) Data–Model Comparison: The baseline and 30 second data and model comparisons are shown in Figures 44 and 45. The data (blue) and models (magenta) values show generally good agreement.

VIII. Discussion

A set of observations to explore the effects of antenna beam patterns and the correction thereof are discussed. These used bright polarized (3C138) or unpolarized (J0408-6545) sources observed with a series of offsets of 0.83° from the pointing center covering various sectors of the beam patterns. The July session of observations included the MeerKAT Extension antenna e121. This antenna has a diameter of 15 m as opposed to the MeerKAT antennas diameter of 13.5 m making its beam pattern significantly narrower than those of the other antennas.

Extended observing sessions were used to allow parallactic angle rotation to make the source illuminate overlapping traces through the beam pattern. These data were then compared with holographic beam images using simple models of the sources. This comparison (Figs. 2-6) shows good agreement.

Antenna pointing errors will shift the location in the beam pattern in which the sources is being observed. The typical MeerKAT blind pointing errors are of the order of an arcmin; reference pointing was used to reduce the effect of these.

The various offset pointings were imaged with and without corrections for the effects of the beam shape. These observations were deliberately designed to cover an extreme case. The antenna power pattern at the middle of L Band at the offset used is about 0.2; further from the beam center than most observations use. This maximizes the effects of the parallactic angle rotation of a single pattern or the differences among various beam patterns. Uncorrected variations in the complex antenna gain in the direction of a source being imaged will result in artifacts in the image derived from such data and potentially an incorrect brightness of true emission. Such defects can be especially severe in polarized emission.

The imaging used Obit program MFBeam which applies corrections for antenna beam patterns in the deconvolution process. The corrections used one array average pattern per antenna design. Comparisons are presented of the images of the offset pointings with and without corrections for the

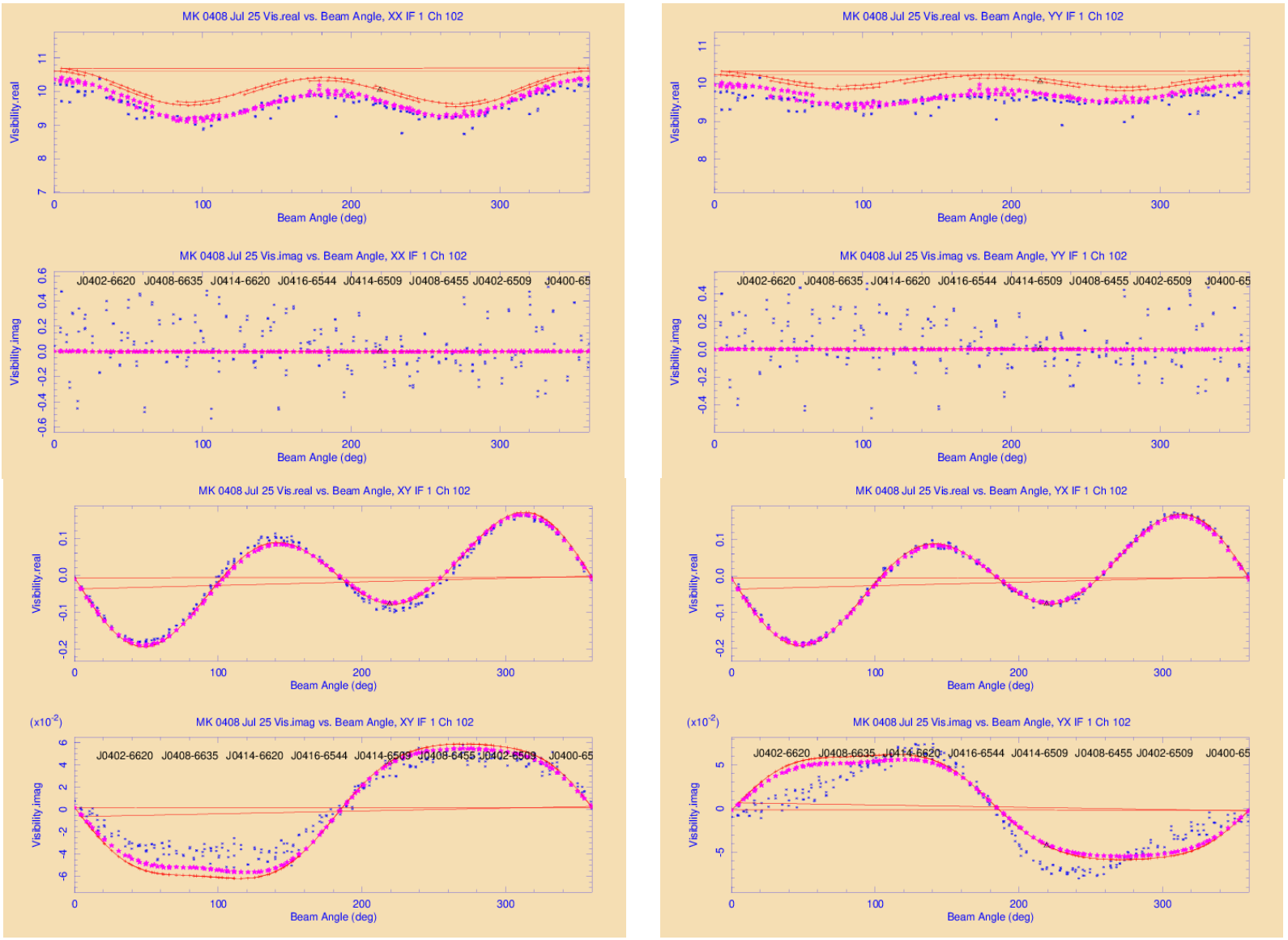

Fig. 7. Like Figure 2 but J0408-6545 reference pointed offset data from 23 July 2025 on baselines amoung MeerKAT antennas. The data are from channel 102 in the first suband(IF), ν=0.928 GHz. Blue *'s are the observed data, the red +s and line are the model calculated from the total flux density and the Beam images. The magenta filled stars are model visibilities generated by UVPolCor using a CLEAN model generated by MFBeam. The pointing names are shown on the imaginary plots centered on the the mean beam angle of the observations for that offset pointing.

various tests. These show the technique applied to be generally effective.

It is notable that the addition of a single MeerKAT Extenson antenna to the 60ish MeerKAT antennas added significant artifacts; the final compliment of 14 such antennas should have a larger effect. The residual image artifacts are due to some combination of 1) residual calibration errors, 2) deviations of the individual antenna patterns from that assumed, 3) variation of the average pattern with observing geometry and/or ambient temperature and 4) residual pointing errors.

In addition to the reduction of off–source artifacts, the repeat ability of image brightness is an important diagnostic. In a given session, the different offsets observe the same source, at the same time, and using the same calibration and the same offset from the pointing center; the corrected results should be the same. The March and July 2025 sessions on 3C138 are good test cases. The source is strongly polarized and unresolved, the recovered peak flux densities in Stokes I, Q and U should be very similar. Tables IV and VI show this to be the case; the RMS variations of the Stokes I image peaks was reduced by a factor of 7 with respect to the uncorrected images and for Stokes Q and U the reduction was between a factor of 50 and 100.

The application of the technique described here should result in images with a symmetric beam pattern which when the gain correction is applied to the images, should produce the correct pixel brightnesses. In the tests presented here, the ground truth is the image derived from the source on-axis which had the same uv-coverage and calibration.

Tests using the offset 3C138 images in I,Q and U did not

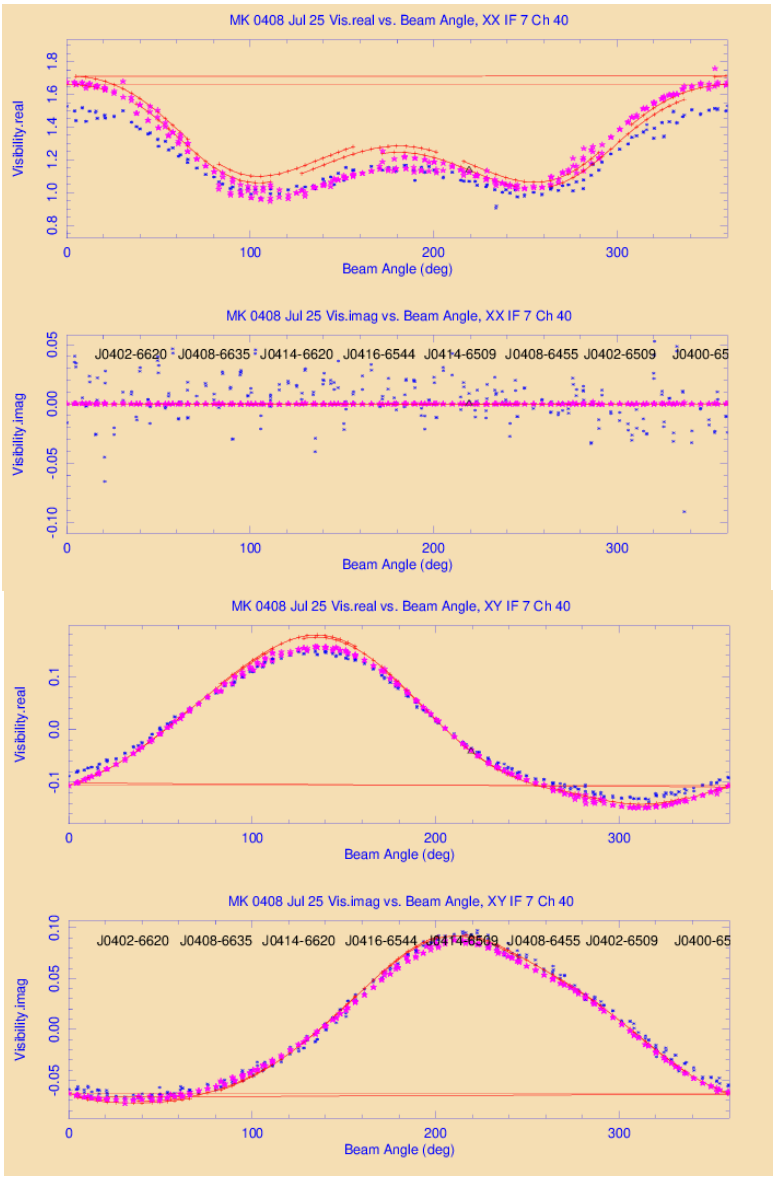

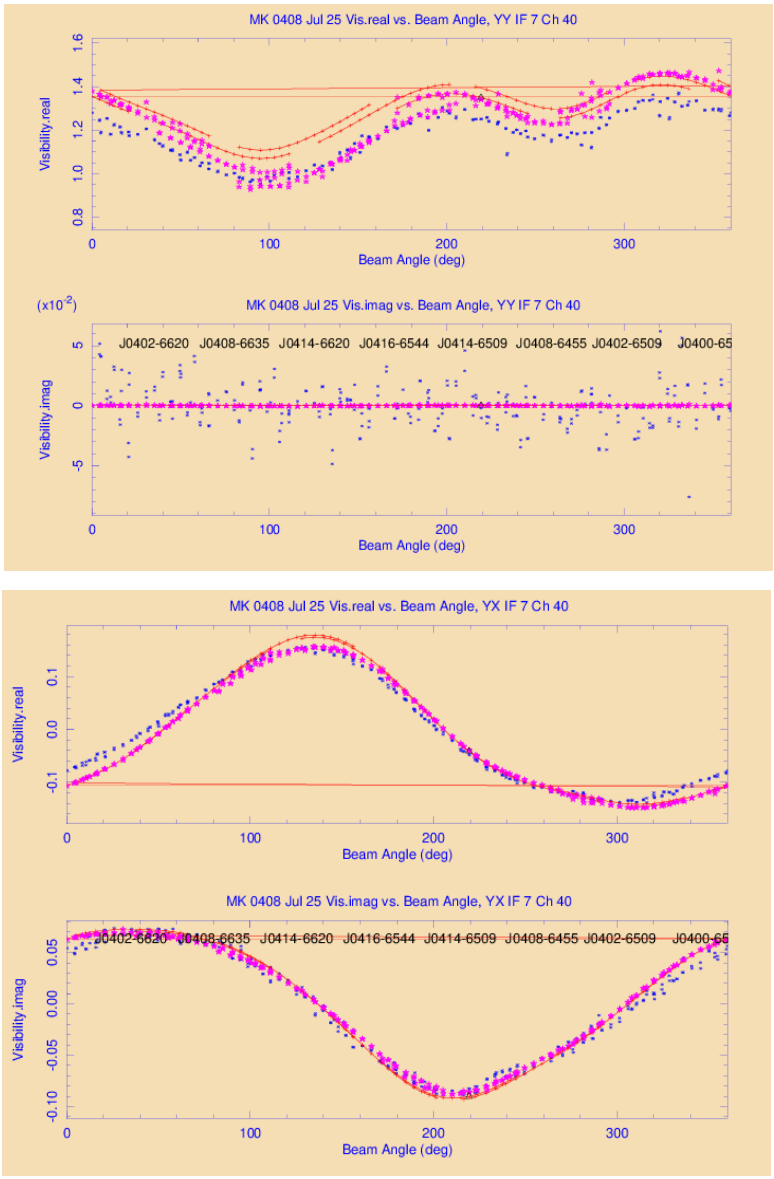

Fig. 8. Like Figure 7 but the data are from channel 40 of 238 in the seventh of eight suband, ν=1.499 GHz.

meet expectations; the recovered flux densities were approximately 15% below the correct value. The same effect was seem in the images derived from the same data but without the beam corrections. The beam correction technique is apparently not responsible for the reduced amplitudes which must be caused by some other aspect of the imaging. Coherence loss due to time and delay smearing is a potential cause. Tests using only shorter baselines (MeerKAT only), hence less prone to time and delay smearing, and with a dataset with no time averaging showed comparable, i.e. low, amplitudes. This is both for the imaging with and without beam corrections. The problem remains unresolved. It should be noted that the conditions used in these tests are far more extreme than will be used in real observation.

There are potential improvements that could be made to what was done in this report. Not all antennas have patterns as close to the average as others, not all point as well as the average. For the analysis presented here only the antenna with really poor pointing (m030 in July) or the worst effect on image artifacts (m049 in July) were excluded. Elimination of more of the poorly performing antennas might help. Another potential issue is how closely the reference pointing center aligns with the center of the beam images. Any misalignment will lead to systematic in image correction.

IX. Acknowledgment

We would like to thank Ludwig Schwardt for invaluable help with the reference pointing.

References

[1] W. D. Cotton and T. Mauch, "Correction of Radio Interferometric Imaging for Antenna Patterns," *PASP*, vol. 133, no. 1028, p. 104502, Oct. 2021.
[2] W. D. Cotton, "Obit: A Development Environment for Astronomical Algorithms," *PASP*, vol. 120, pp. 439–448, 2008.

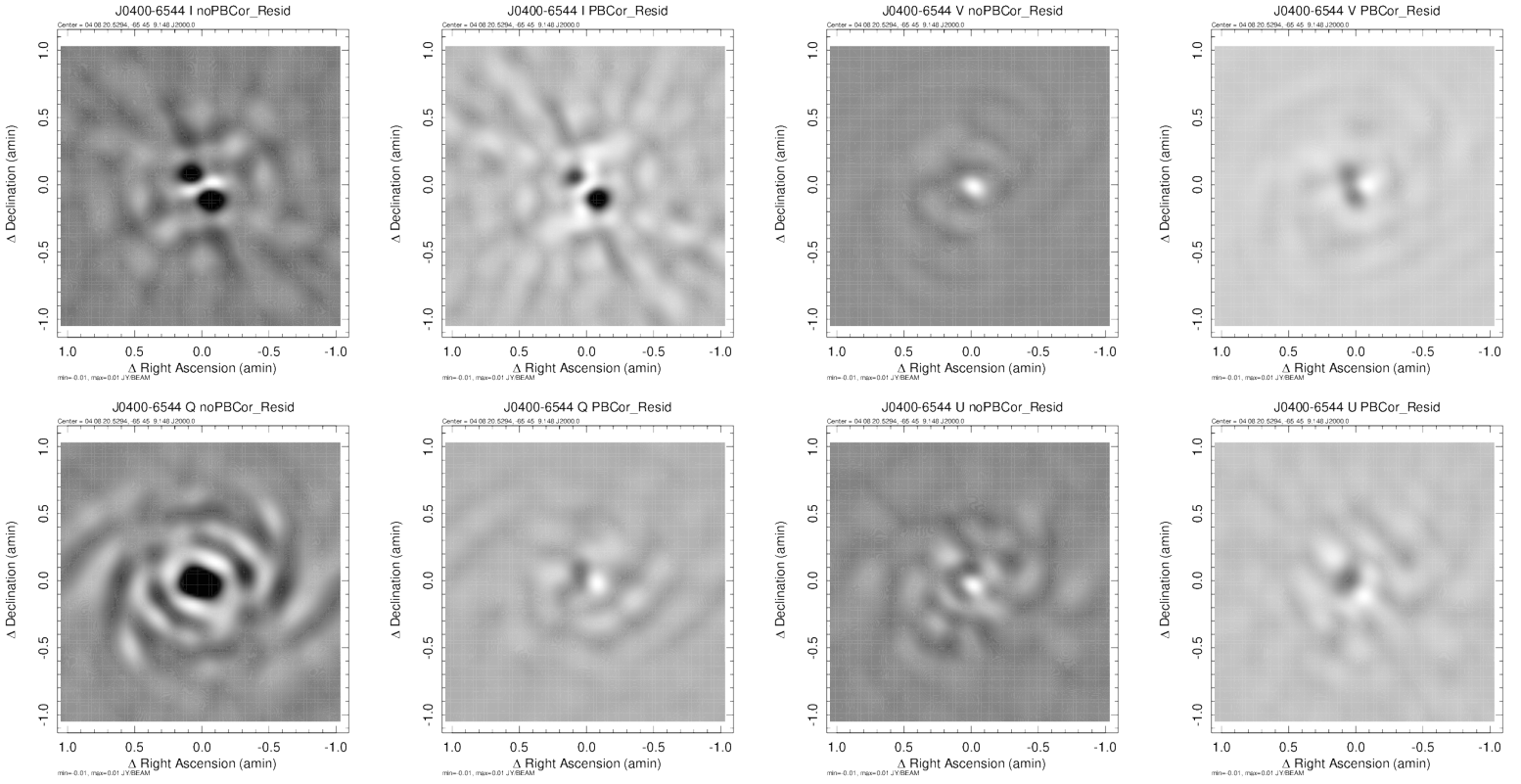

Fig. 9. Offset J0400-6544 Broadband residuals, pair without (left) and with (right) beam corrections. Top row Stokes I (left) and V (right), bottom row Q (left) and U (right). The pixel range displayed is ± 10 mJy/beam. CLEAN was restricted to a single 3 pixel radius circular box centered on the source position and components subtracted were not restored to the image.

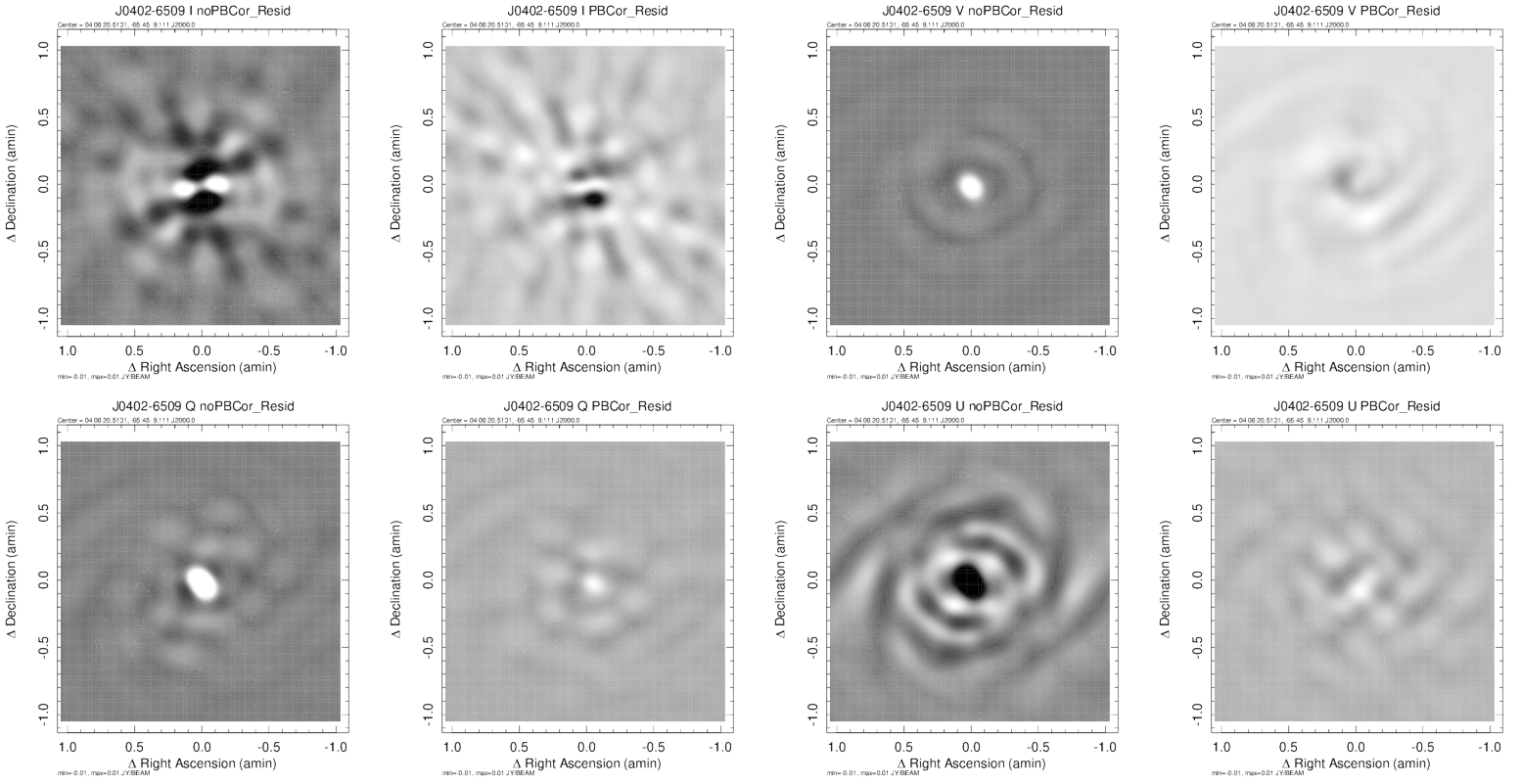

Fig. 10. Like Figure 9 but for J0402-6509. MK only.

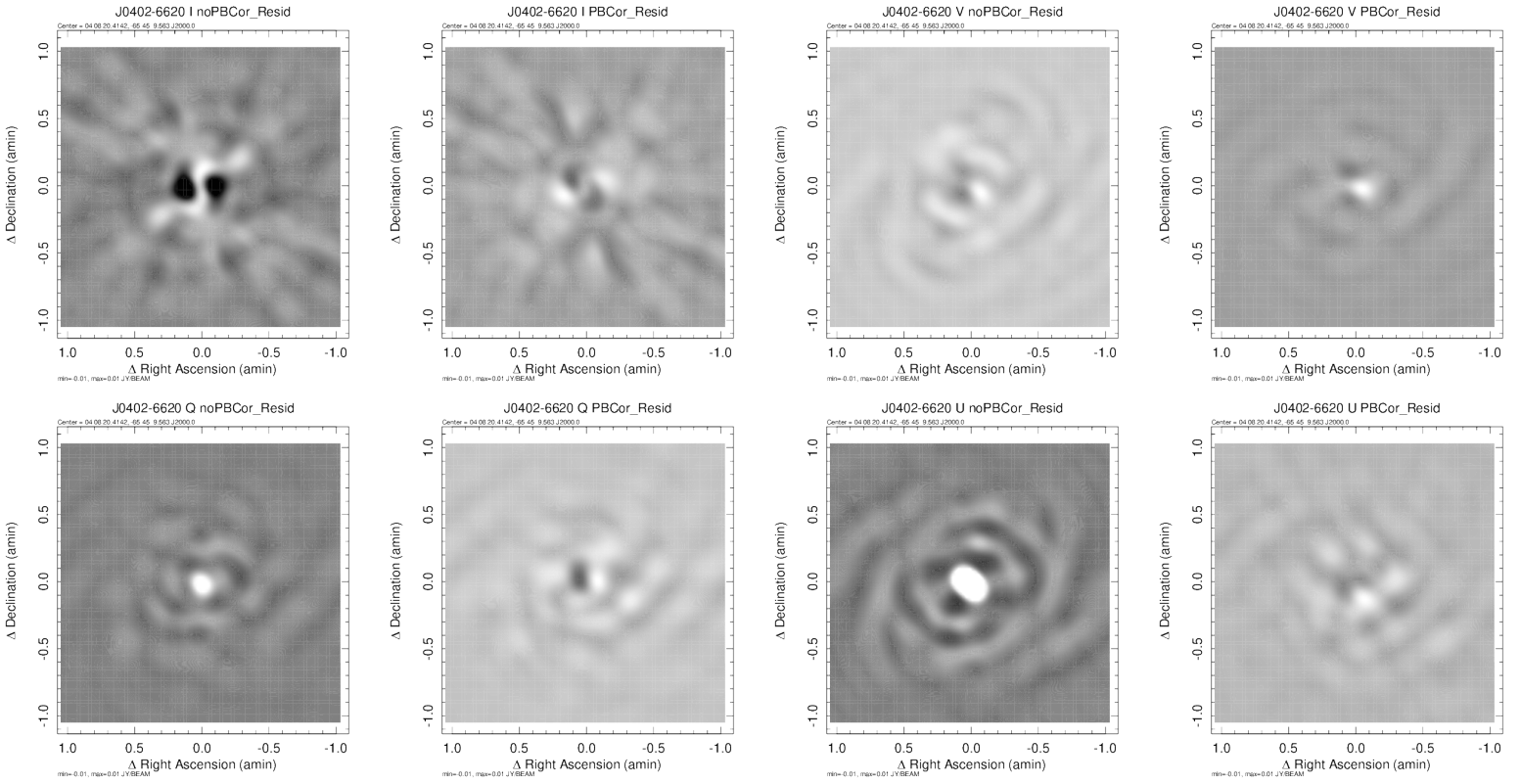

Fig. 11. Like Figure 9 but for J0402-6620. MK only.

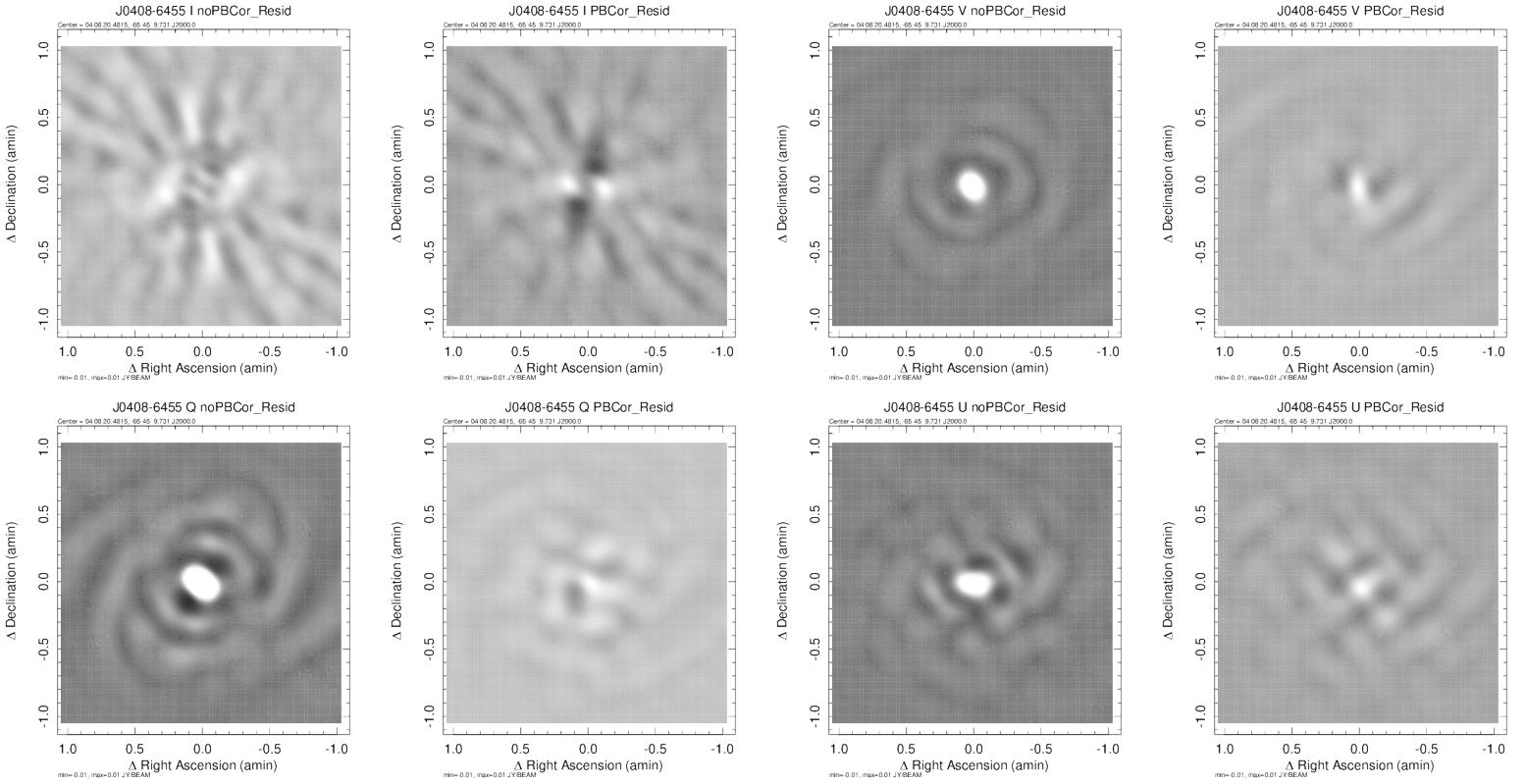

Fig. 12. Like Figure 9 but for J0408-6455. MK only.

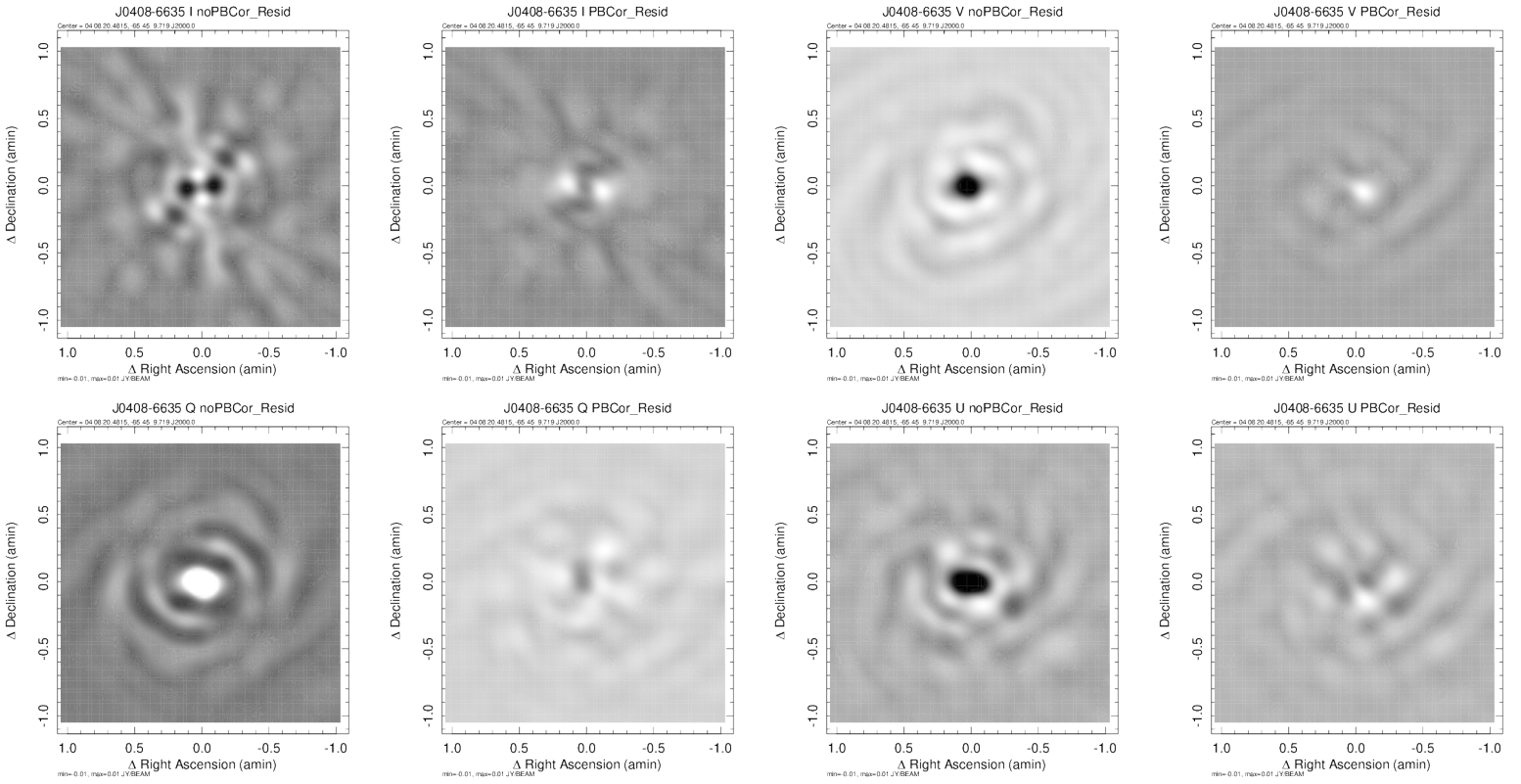

Fig. 13. Like Figure 9 but for J0408-6635. MK only.

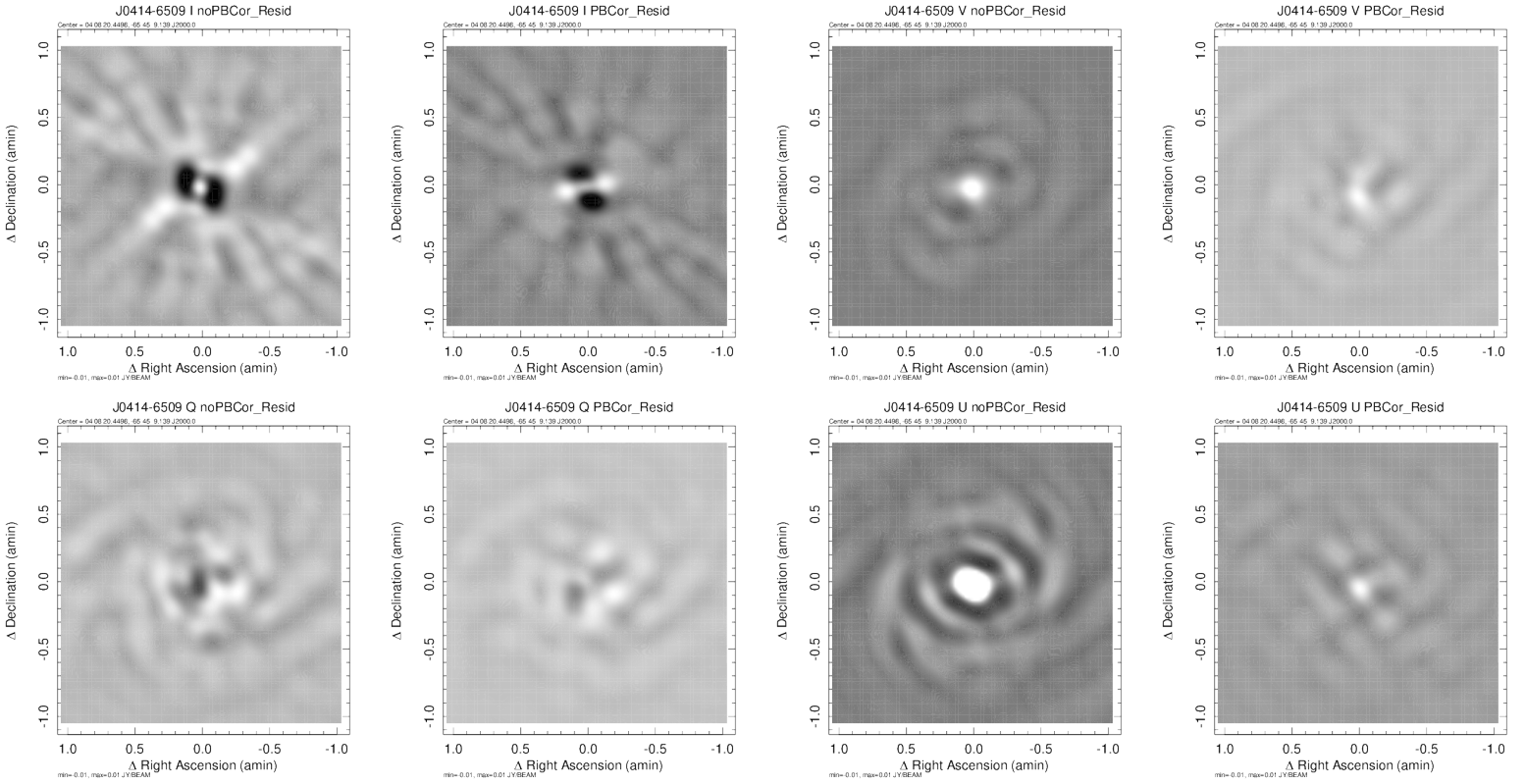

Fig. 14. Like Figure 9 but for J0414-6509. MK only.

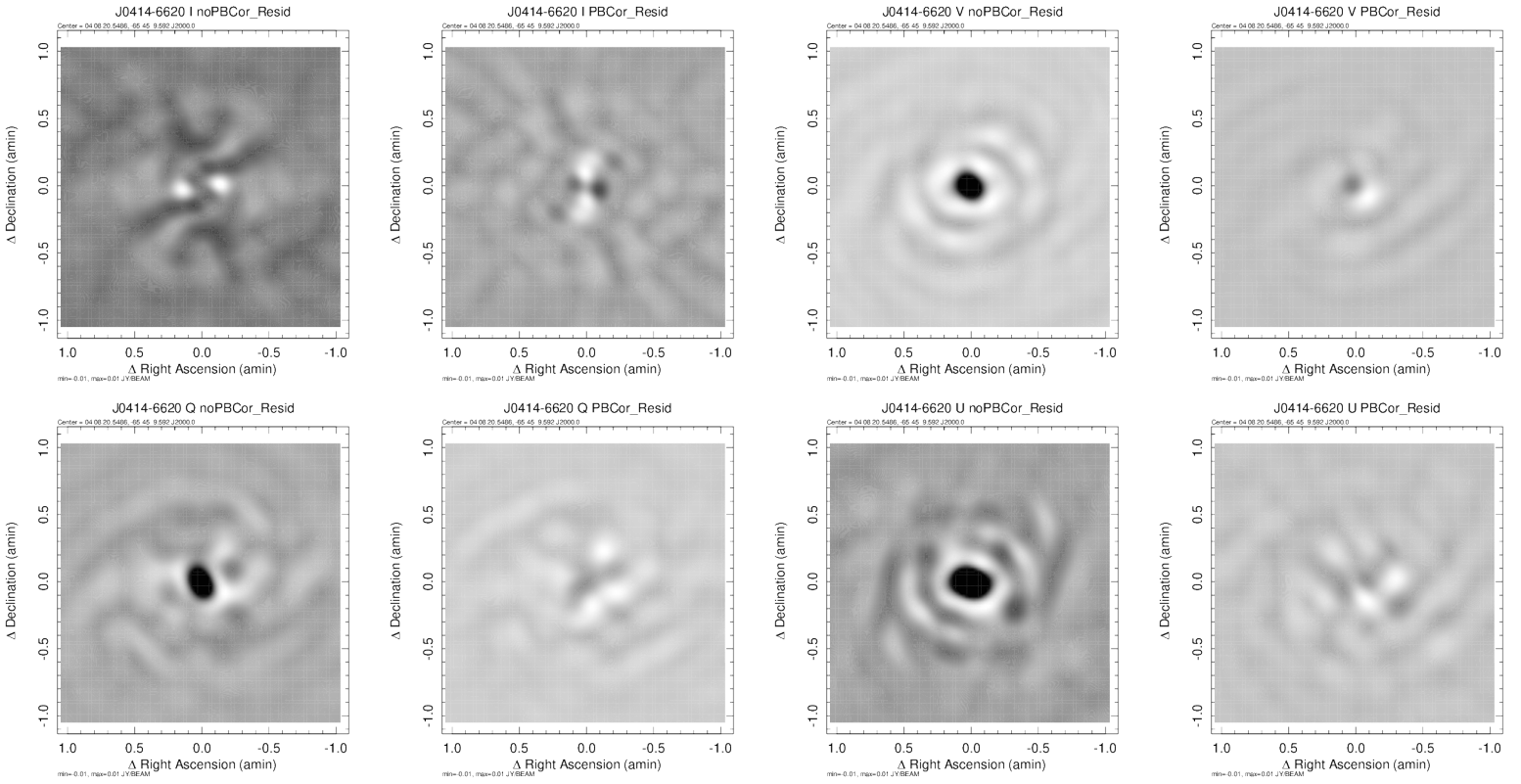

Fig. 15. Like Figure 9 but for J0414-6620. MK only.

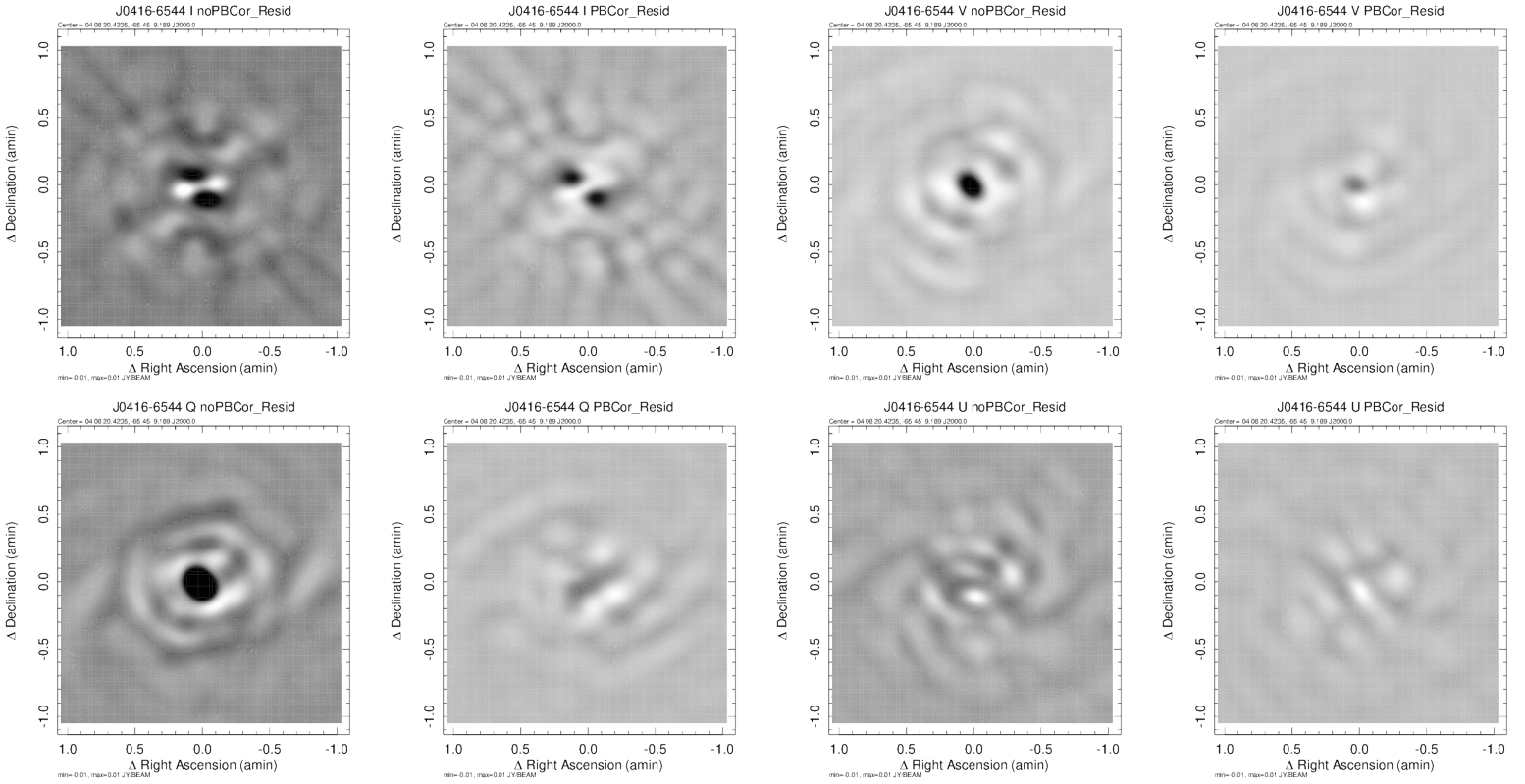

Fig. 16. Like Figure 9 but for J0416-6544. MK only.

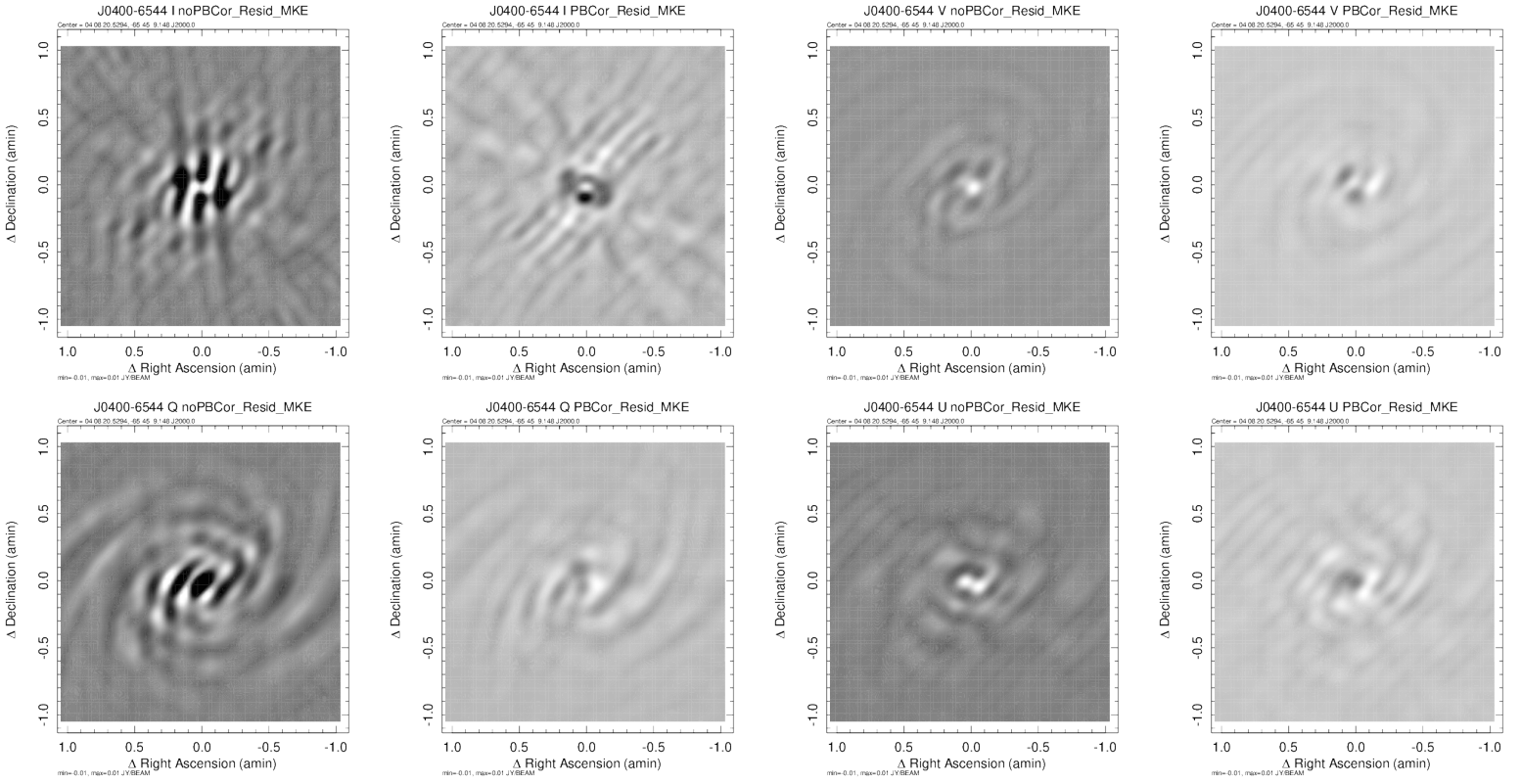

Fig. 17. J0400-6544 Broadband residuals from MeerKAT plus MeerKAT Extension data, pairs without (left) and with (right) beam corrections. CLEAN was restricted to a single 3 pixel radius circular box centered on the source position and components subtracted were not restored to the image. Top row Stokes I (left) and V (right), bottom row Q (left) and U (right). The pixel range displayed is ± 10 mJy/beam.

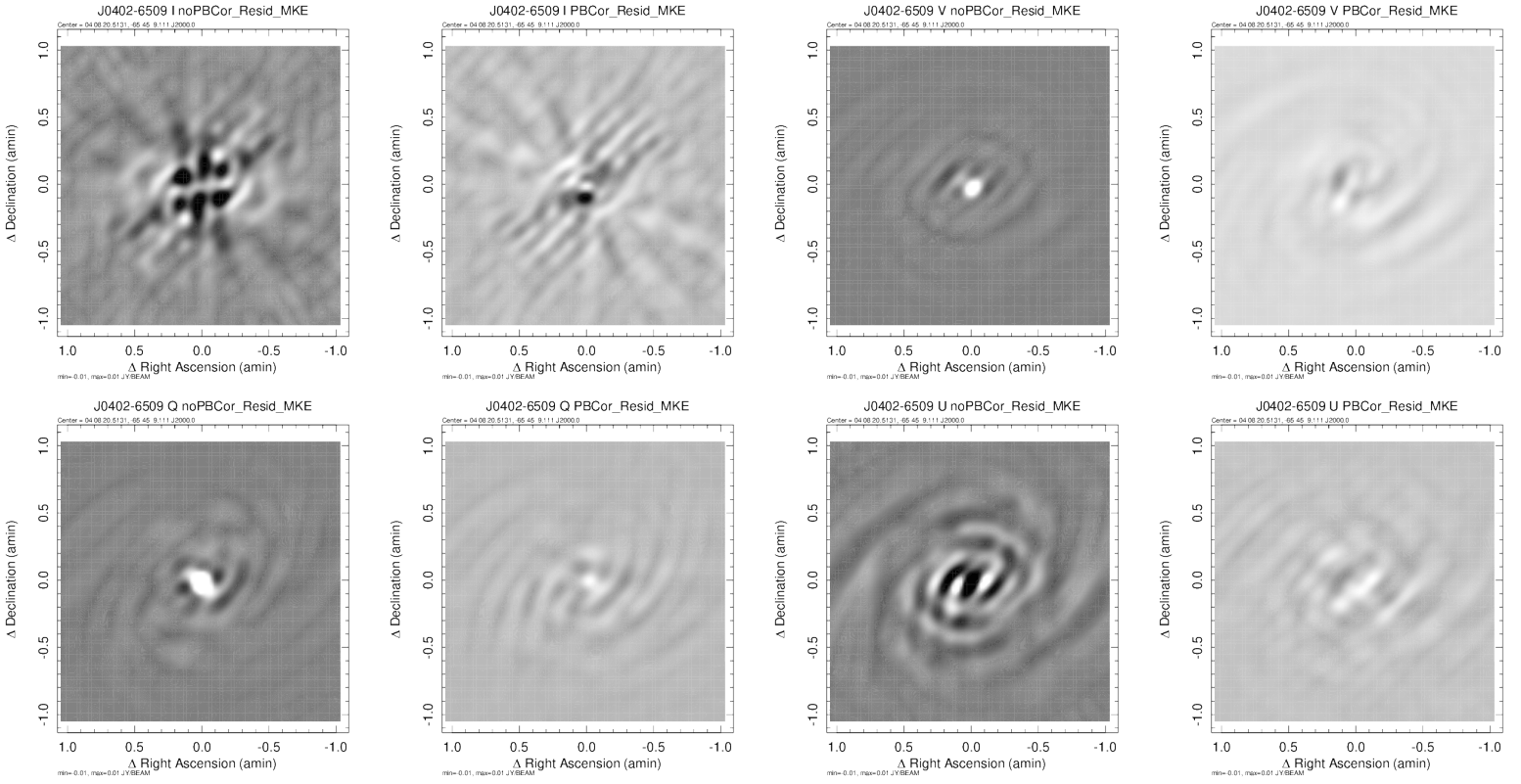

Fig. 18. Like Figure 17 but for J0402-6509, MK+MKE.

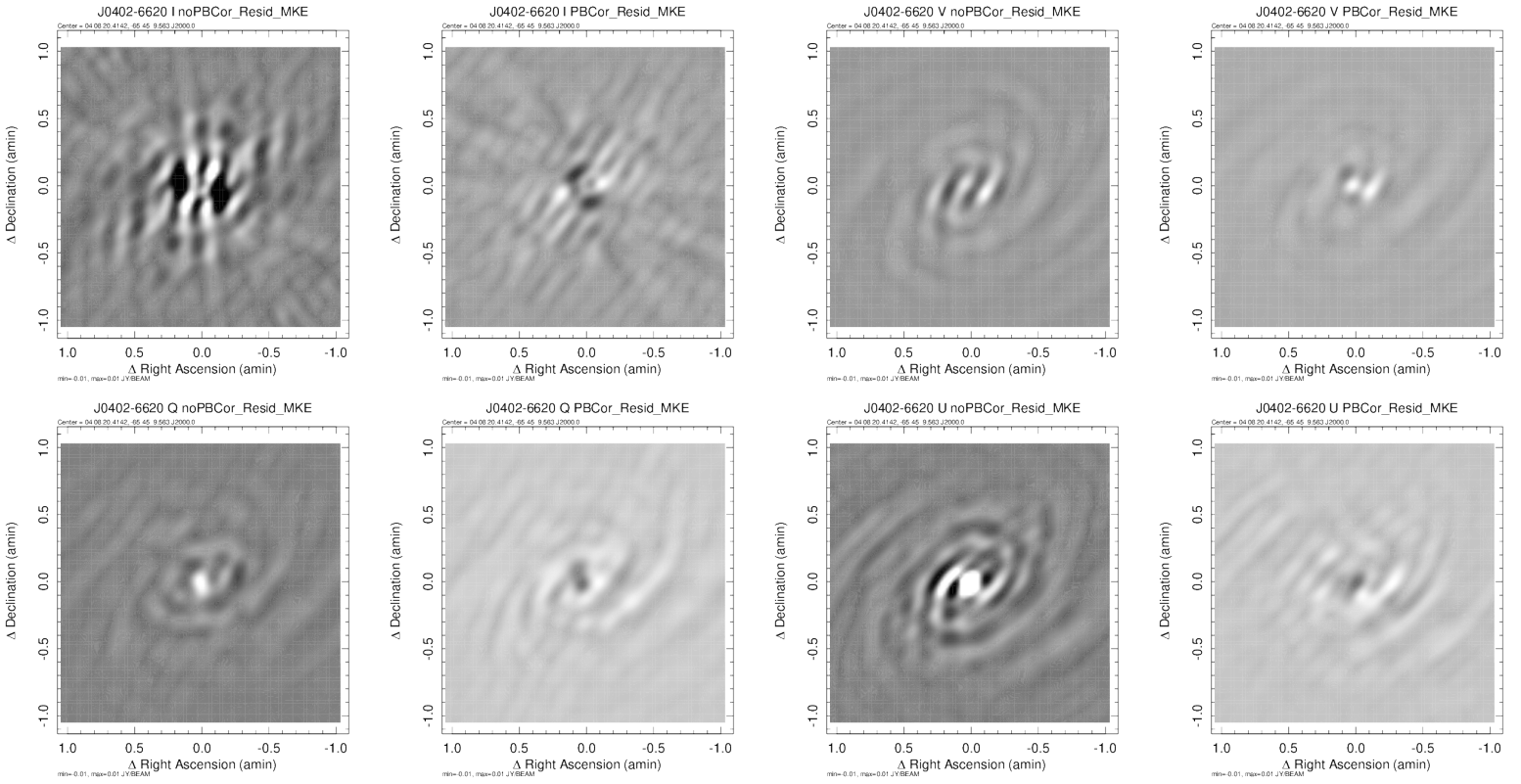

Fig. 19. Like Figure 17 but for J0402-6620, MK+MKE.

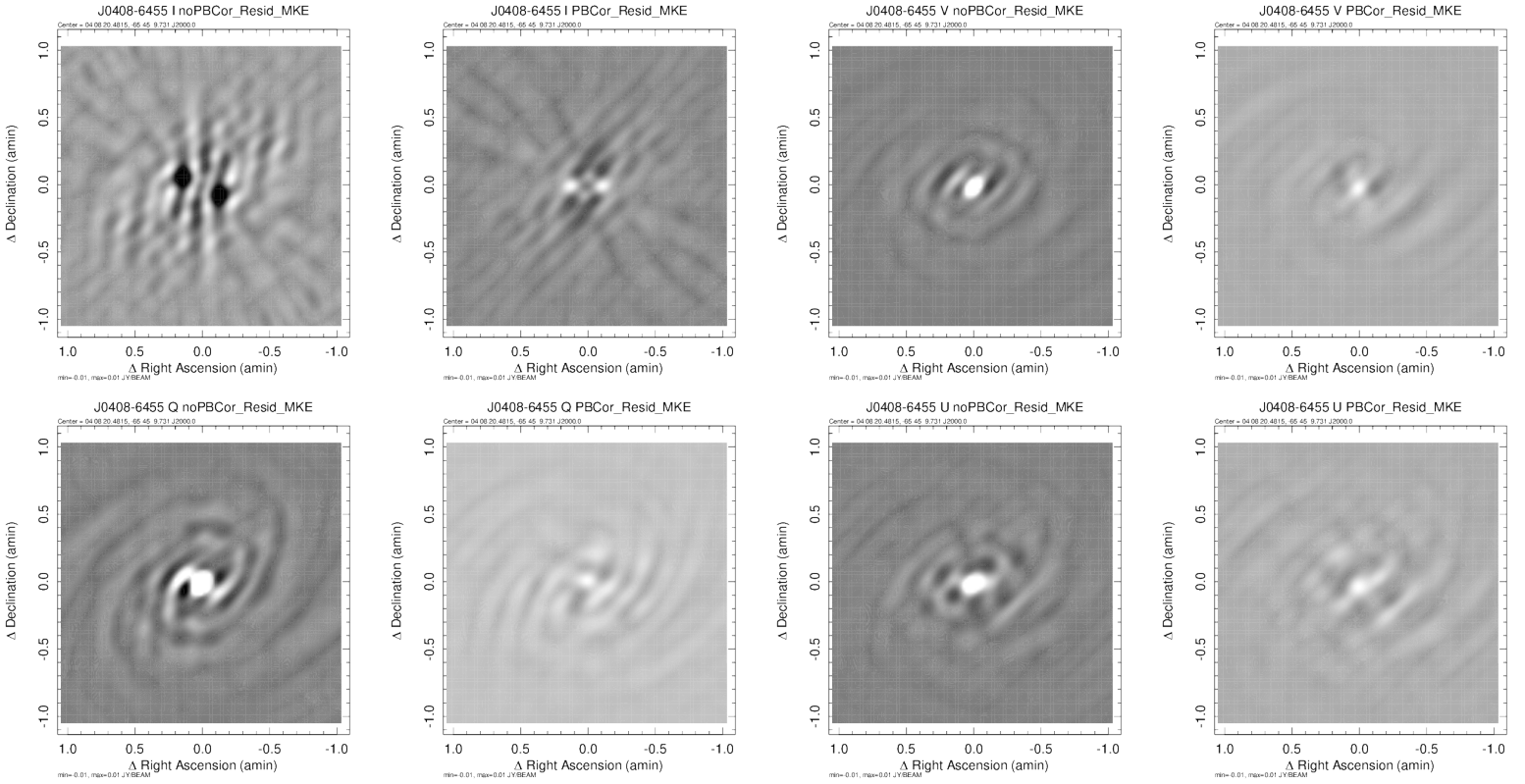

Fig. 20. Like Figure 17 but for J0408-6455, MK+MKE.

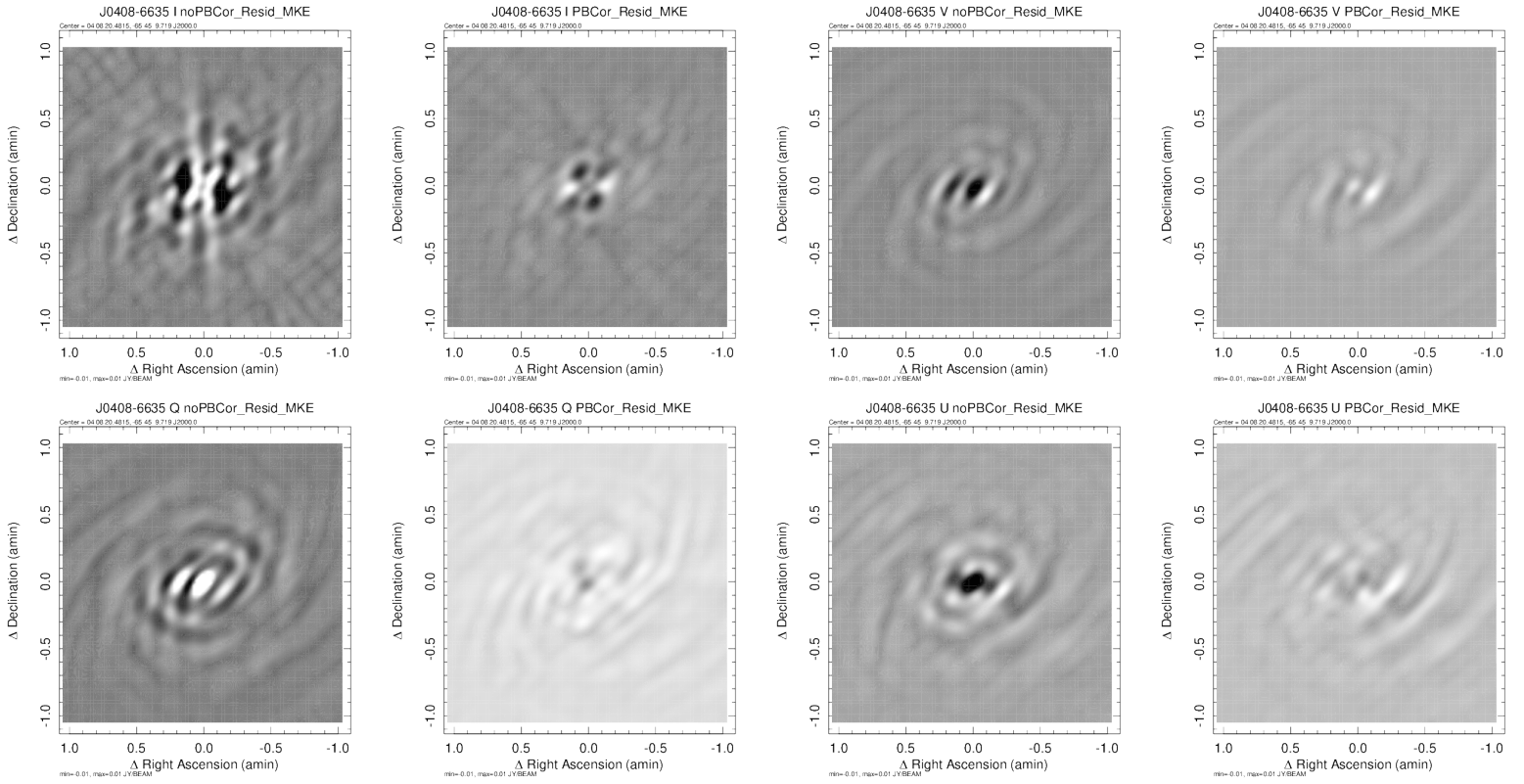

Fig. 21. Like Figure 17 but for J0408-6635, MK+MKE.

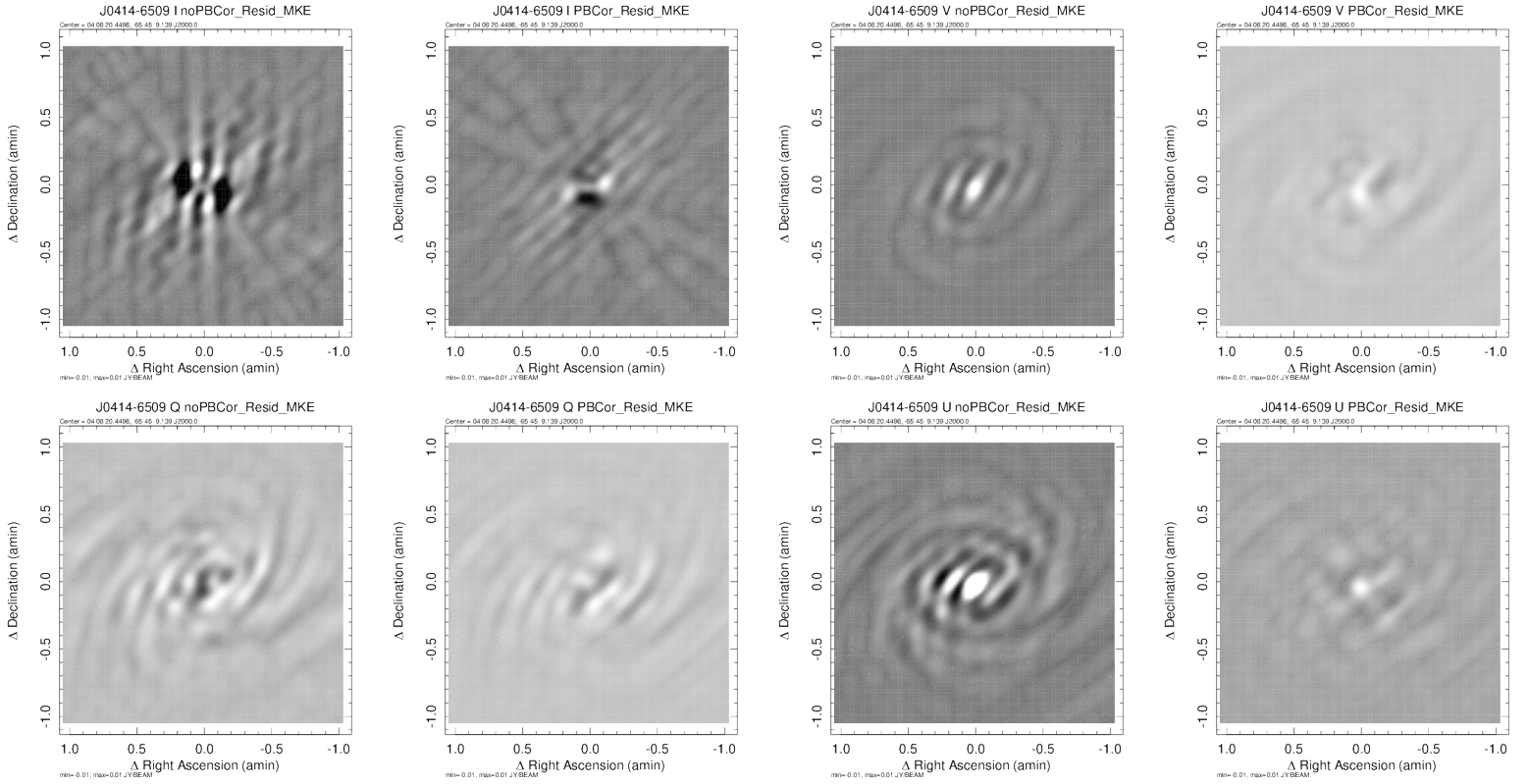

Fig. 22. Like Figure 17 but for J0414-6509, MK+MKE.

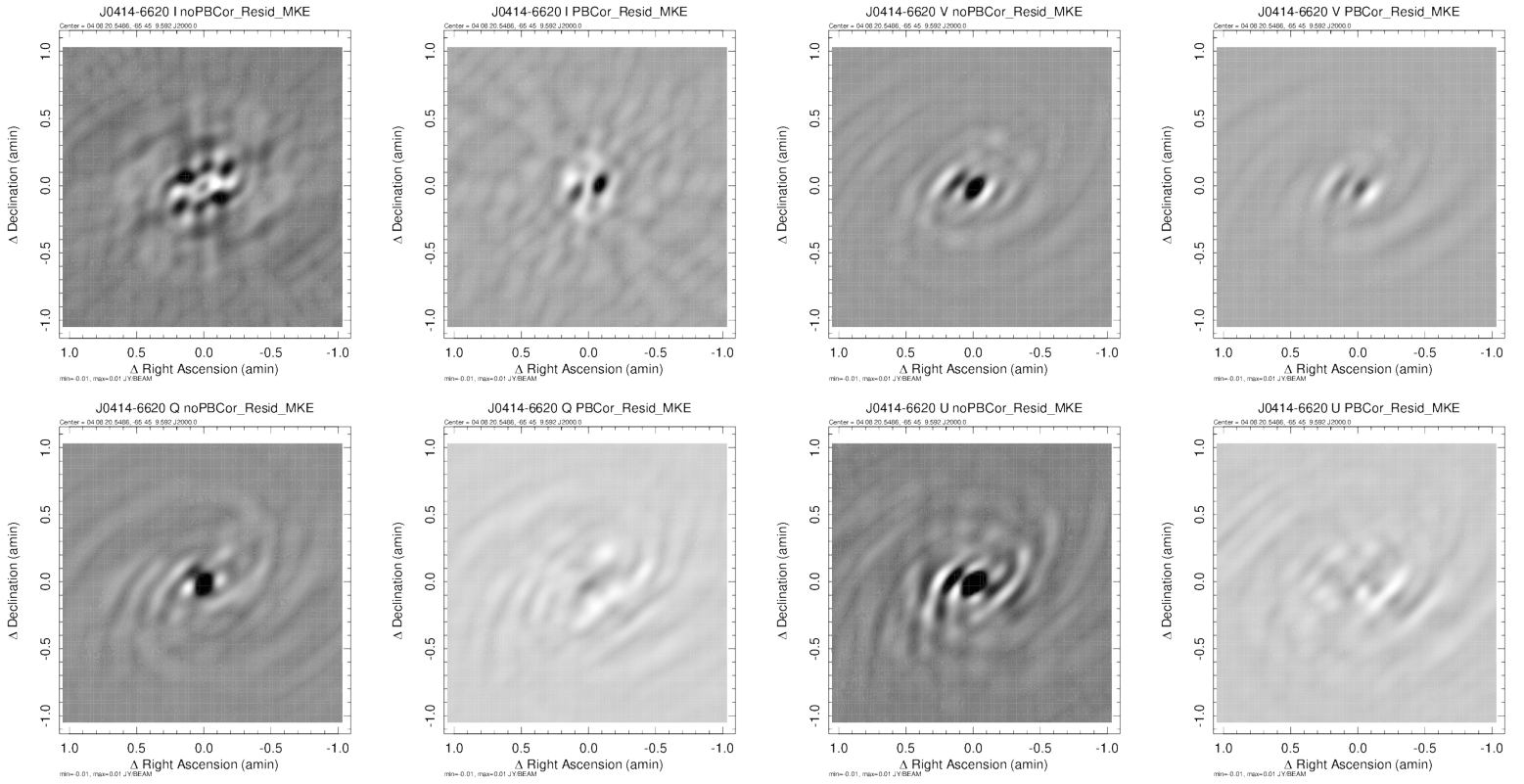

Fig. 23. Like Figure 17 but for J0414-6620, MK+MKE.

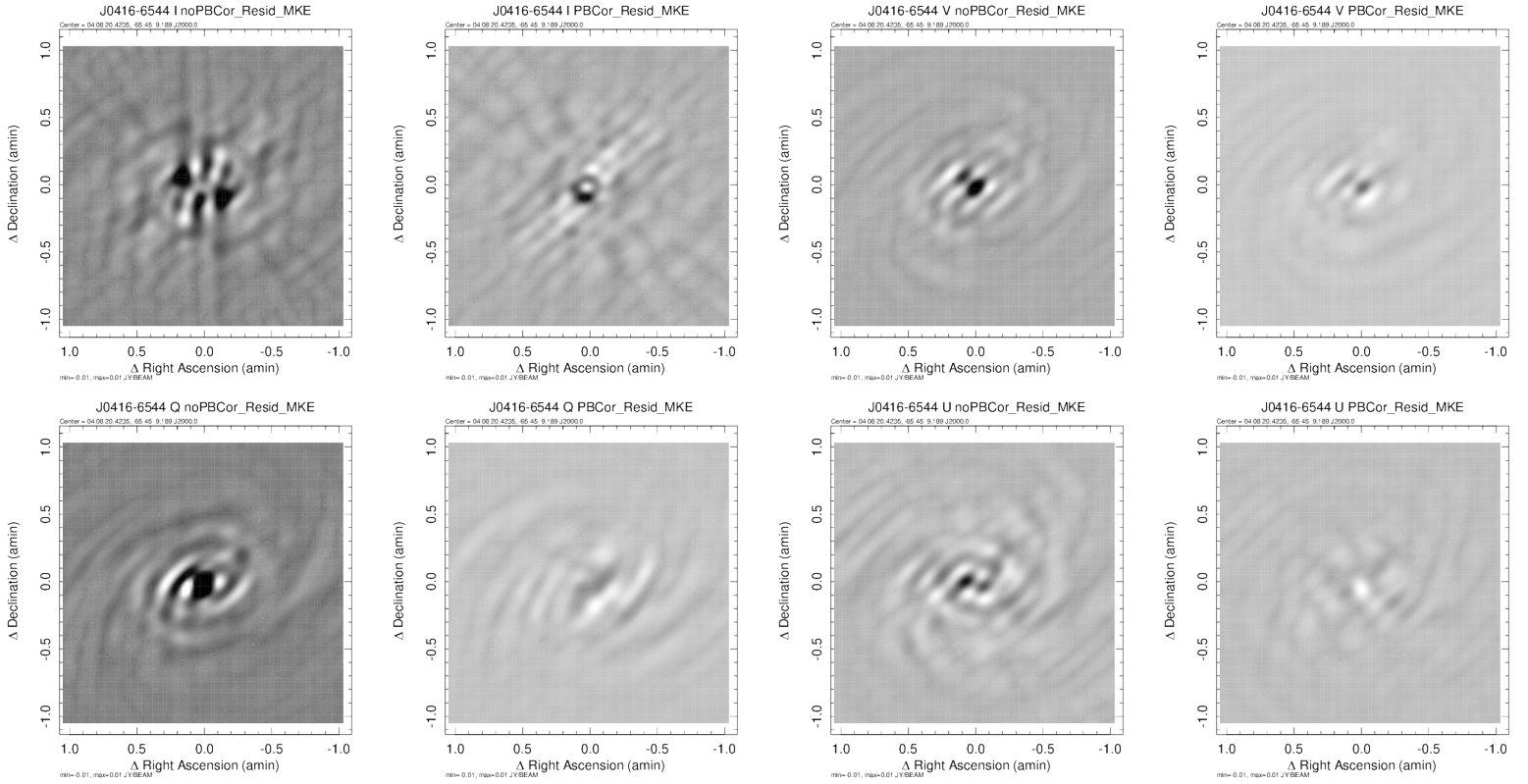

Fig. 24. Like Figure 17 but for J0416-6544.

TABLE IV
EXTREMA MARCH 2025, 3C138

Pointing	I	I PBC	Q	Q PBC	U	U PBC	V	V PBC
J0518+1638	+1.26873	+1.25346	-0.01060	+0.04541	-0.07716	-0.08805	-0.01041	+0.00485
J0519+1603	+1.30174	+1.26479	+0.06018	+0.04703	-0.03368	-0.08594	-0.01656	+0.00421
J0519+1714	+1.47451	+1.30817	+0.04663	+0.05210	-0.14237	-0.08428	+0.00422	+0.00685
J0521+1548	+1.37473	+1.22101	+0.11521	+0.05472	-0.06411	-0.07966	-0.00703	+0.00433
J0521+1728	+1.50931	+1.25618	+0.08726	+0.05233	-0.12005	-0.07829	+0.01292	+0.00473
J0524+1603	+1.29599	+1.18927	+0.05848	+0.05976	-0.11573	-0.07994	+0.01276	+0.00728
J0524+1714	+1.37625	+1.24012	+0.03657	+0.05200	-0.06308	-0.08256	+0.01730	+0.00396
J0525+1638	+1.23498	+1.21481	-0.01162	+ 0.05695	-0.10379	-0.08524	+0.01564	+0.00686
RMS	0.004194	0.000574	0.000840	0.000010	0.000577	0.000005	0.000076	0.000076

Notes:
Columns are labeled with the Stokes parameter.
Columns labeled "PBC" are values from beam corrected images, others are uncorrected.
The "RMS" row is the root mean square of the values in that column.

TABLE V
GAIN CORRECTED PEAK MARCH 2025, 3C138, MEERKAT ONLY

Pointing	I	I PBC	Q	Q PBC	U	U PBC
Center	9.02	9.02	0.346	0.346	-0.472	-0.472
J0518+1638	7.56	7.77	0.073	0.257	-0.453	-0.475
J0519+1603	7.66	7.82	0.383	0.277	-0.193	-0.464
J0519+1714	8.44	8.01	0.249	0.282	-0.806	-0.450
J0521+1548	8.29	7.67	0.627	0.311	-0.452	-0.405
J0521+1728	8.57	7.76	0.413	0.287	-0.635	-0.413
J0524+1603	7.65	7.41	0.371	0.330	-0.799	-0.403
J0524+1714	7.95	7.63	0.210	0.299	-0.358	-0.459
J0525+1638	7.30	7.58	0.042	0.323	-0.619	-0.479
Off. Avg	7.93	7.71	0.296	0.296	-0.539	-0.443
Ratio	0.88	0.85	0.856	0.857	1.142	0.939

Notes:
Columns are labeled with the Stokes parameter. Offset pointing values have been corrected by the gain (0.1955).
The "Center" row contains values from the pointing centered on J0521+1638.
Columns labeled "PBC" are values from beam corrected images, others are uncorrected.
The "Off. Avg" row contains the average of the offset pointing values in that column.
The "Ratio" row contains the ratio of average of the offset pointing values in that column to the center pointing value.

[3] ——, "MeerKAT Continuum Scripts: Outline of Data Reduction and Heuristics," *Obit Development Memo Series*, vol. 90, pp. 1–30, 2025. [Online]. Available: https://www.cv.nrao.edu/ bcotton/ObitDoc/MKObitScripts.pdf
[4] W. D. Cotton, J. J. Condon, K. I. Kellermann, M. Lacy, R. A. Perley, A. M. Matthews, T. Vernstrom, D. Scott, and J. V. Wall, ""The Angular Size Distribution of μjy Radio S"ources"," *ApJ*, vol. 856, p. 67, 2018.
[5] W. D. Cotton, "Cross Polarized Delay Calibration of Linear Feeds with XYDly and General Polarization Calibration," *Obit Development Memo Series*, vol. 89, pp. 1–8, 2025. [Online]. Available: https://www.cv.nrao.edu/ bcotton/ObitDoc/XYDly.pdf

TABLE VI
EXTREMA JULY 2025, 3C138

Pointing	I	I PBC	Q	Q PBC	U	U PBC	V	V PBC
J0518+1638	+1.0708	+1.0435	+0.0106	+0.0486	-0.0558	-0.0632	-0.0155	+0.0034
J0519+1603	+1.0979	+1.0423	+0.0572	+0.0506	-0.0170	-0.0614	-0.0143	+0.0030
J0519+1714	+1.2390	+1.0921	+0.0505	+0.0527	-0.1136	-0.0592	-0.0078	+0.0037
J0521+1548	+1.1679	+1.0340	+0.1057	+0.0557	-0.0508	-0.0608	-0.0039	+0.0037
J0521+1728	+1.3209	+1.0716	+0.0964	+0.0539	-0.0972	-0.0579	+0.0038	+0.0027
J0524+1603	+1.1654	+1.1149	+0.0624	+0.0648	-0.0949	-0.0720	+0.0092	+0.0036
J0524+1714	+1.1962	+1.0374	+0.0516	+0.0528	-0.0418	-0.0590	+0.0125	-0.0021
J0525+1638	+1.0508	+1.0004	+0.0089	+0.0552	-0.0813	-0.062	0 +0.0132	+0.0033
RMS	0.003573	0.000579	0.000529	0.000010	0.000473	0.000009	0.000059	0.000059

Notes:
Columns are labeled with the Stokes parameter.
Columns labeled "PBC" are values from beam corrected images, others are uncorrected.
The "RMS" row is the root mean square of the values in that column.

TABLE VII
GAIN CORRECTED PEAK JULY 2025, 3C138, MK+MKE

Pointing	I	I PBC	Q	Q PBC	U	U PBC
Center	8.31	8.31	0.371	0.371	-0.391	-0.391
J0518+1638	6.71	6.97	0.085	0.287	-0.287	-0.291
J0519+1603	6.76	6.89	0.359	0.301	-0.049	-0.279
J0519+1714	7.45	7.12	0.268	0.296	-0.568	-0.274
J0521+1548	7.24	6.86	0.589	0.322	-0.294	-0.267
J0521+1728	7.72	7.03	0.471	0.303	-0.459	-0.267
J0524+1603	6.95	7.02	0.375	0.347	-0.515	-0.315
J0524+1714	7.19	6.87	0.267	0.307	-0.233	-0.280
J0525+1638	6.57	6.73	0.100	0.327	-0.400	-0.285
Off. Avg	7.07	6.94	0.314	0.311	-0.351	-0.282
Ratio	0.85	0.83	0.846	0.838	0.896	0.722

Notes:
Columns are labeled with the Stokes parameter. Offset pointing values have been corrected by the gain (0.1955).
The "Center" row contains values from the pointing centered on J0521+1638.
Columns labeled "PBC" are values from beam corrected images, others are uncorrected.
The "Off. Avg" row contains the average of the offset pointing values in that column.
The "Ratio" row contains the ratio of average of the offset pointing values in that column to the center pointing value.

TABLE VIII
GAIN CORRECTED PEAK JULY 2025, 3C138, MK+MKE, NO AVG.

Pointing	I	I PBC	Q	Q PBC	U	U PBC
Center	8.31	8.31	0.368	0.368	-0.393	-0.393
J0518+1638	4.77	4.99	0.107	0.289	-0.303	-0.303
J0519+1603	4.37	4.83	0.362	0.301	-0.078	-0.292
J0519+1714	6.28	6.25	0.267	0.294	-0.591	-0.283
J0521+1548	4.55	4.62	0.586	0.320	-0.301	-0.273
J0521+1728	5.60	5.42	0.480	0.305	-0.465	-0.276
J0524+1603	4.75	5.28	0.356	0.338	-0.542	-0.293
J0524+1714	5.87	5.29	0.268	0.311	-0.229	-0.292
J0525+1638	4.34	4.71	0.113	0.334	-0.408	-0.295
Off. Avg	5.07	5.18	0.318	0.312	-0.364	-0.288
Ratio	0.61	0.62	0.864	0.847	0.928	0.734

Notes:
Columns are labeled with the Stokes parameter. Offset pointing values have been corrected by the gain (0.1955).
The “Center” row contains values from the pointing centered on J0521+1638.
Columns labeled “PBC” are values from beam corrected images, others are uncorrected.
The “Off. Avg” row contains the average of the offset pointing values in that column.
The “Ratio” row contains the ratio of average of the offset pointing values in that column to the center pointing value.

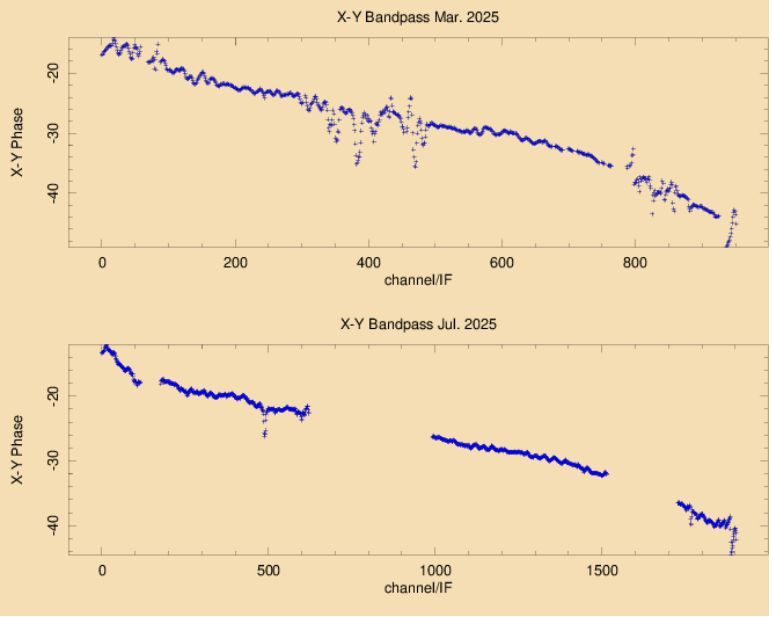

Fig. 25. The X-Y Phase residual spectrum derived for the March 2025 observation (upper panel). and July 2025 (lower panel). The reference antenna for both was m059. The channel width in the July data is half that in the March data.

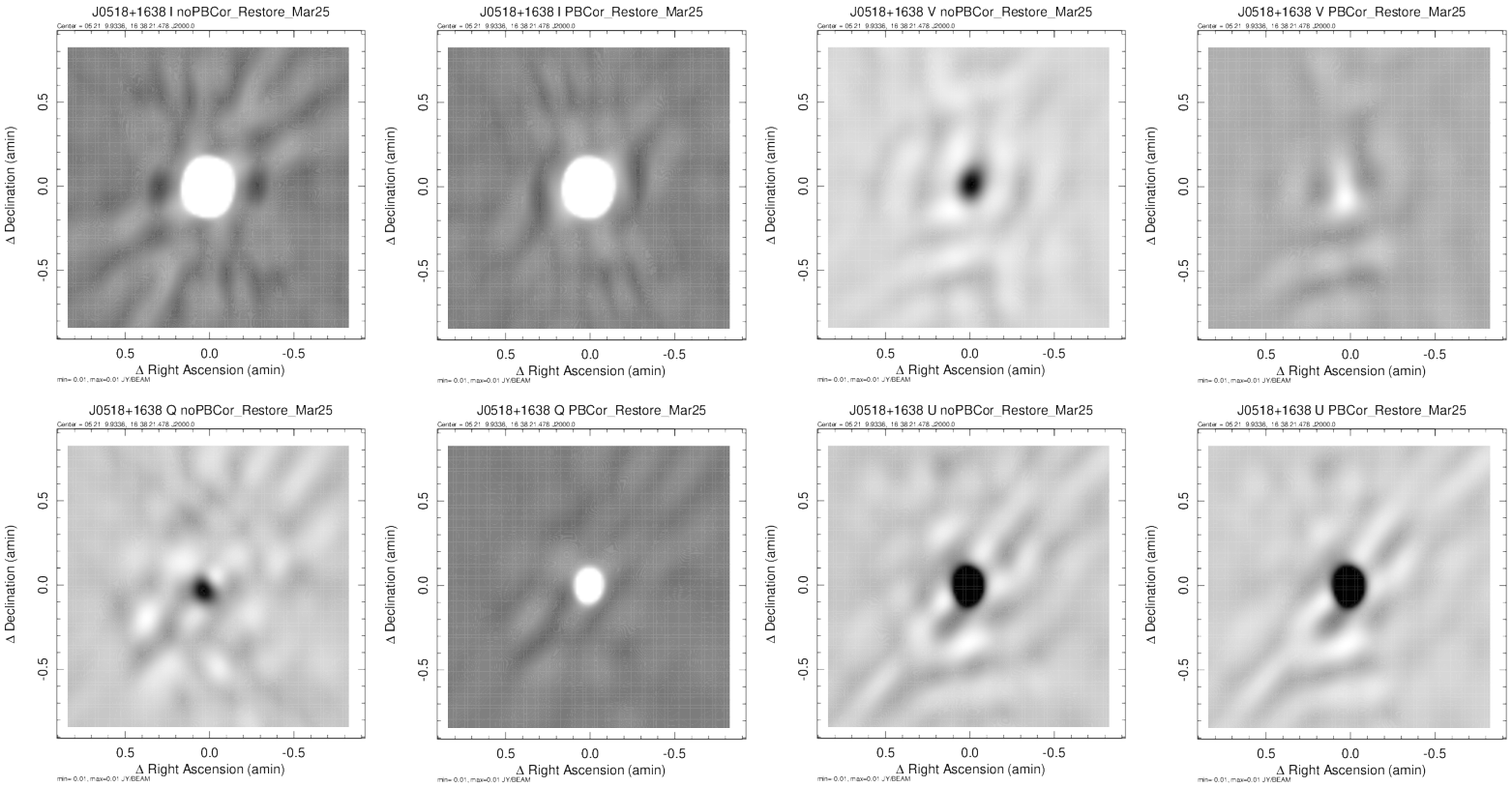

Fig. 26. J0518+1638 Broadband images from MeerKAT only offset pointings of 3C138 from 03 March 2025 as pairs without (left) and with (right) beam corrections. CLEAN was restricted to a single 3 pixel radius circular box centered on the source position and boxes on two nearby sources. to the image. Top row Stokes I (left) and V (right), bottom row Q (left) and U (right). The pixel range displayed is $\pm$10 mJy/beam.

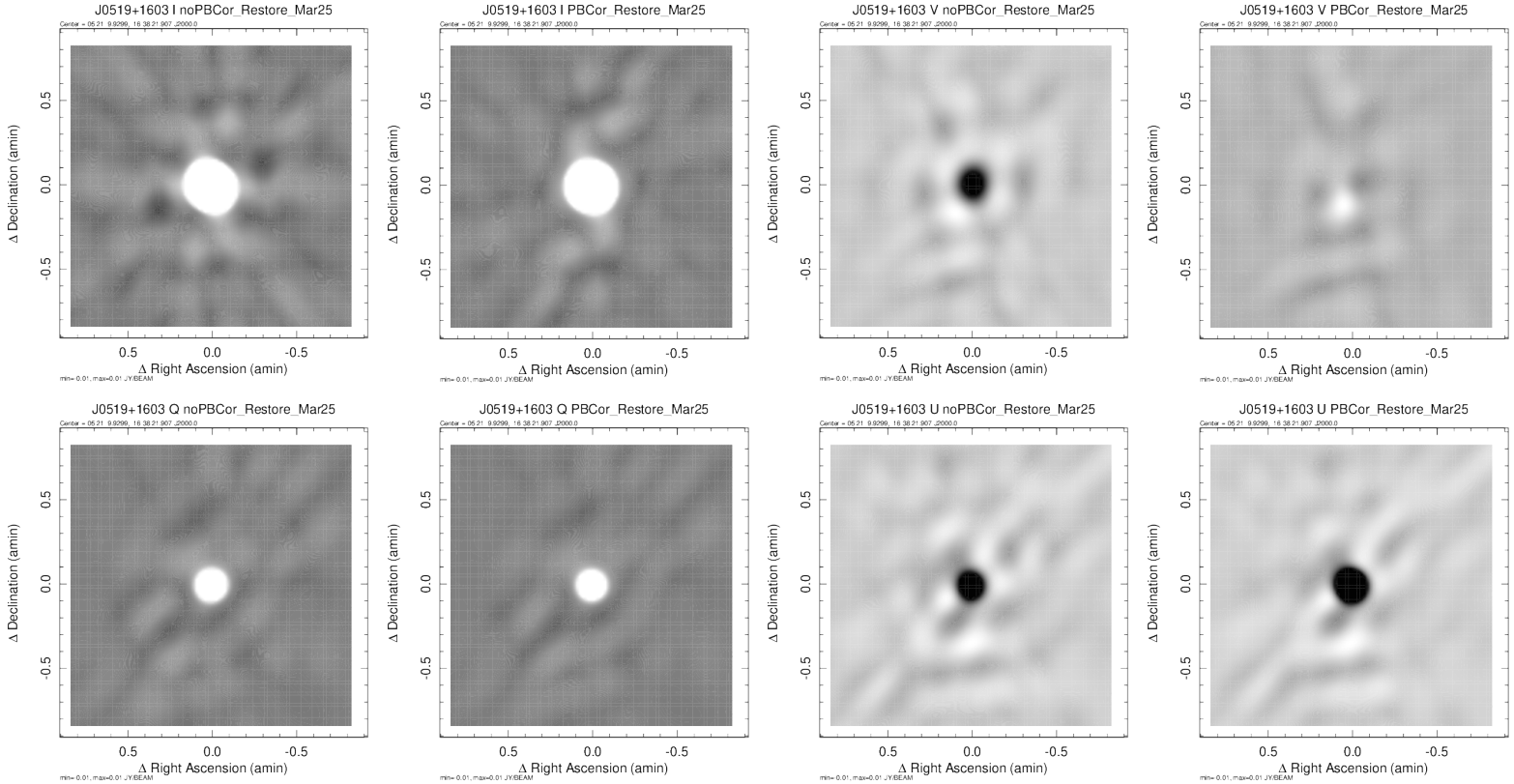

Fig. 27. Like Figure 26 but for J0519+1603.

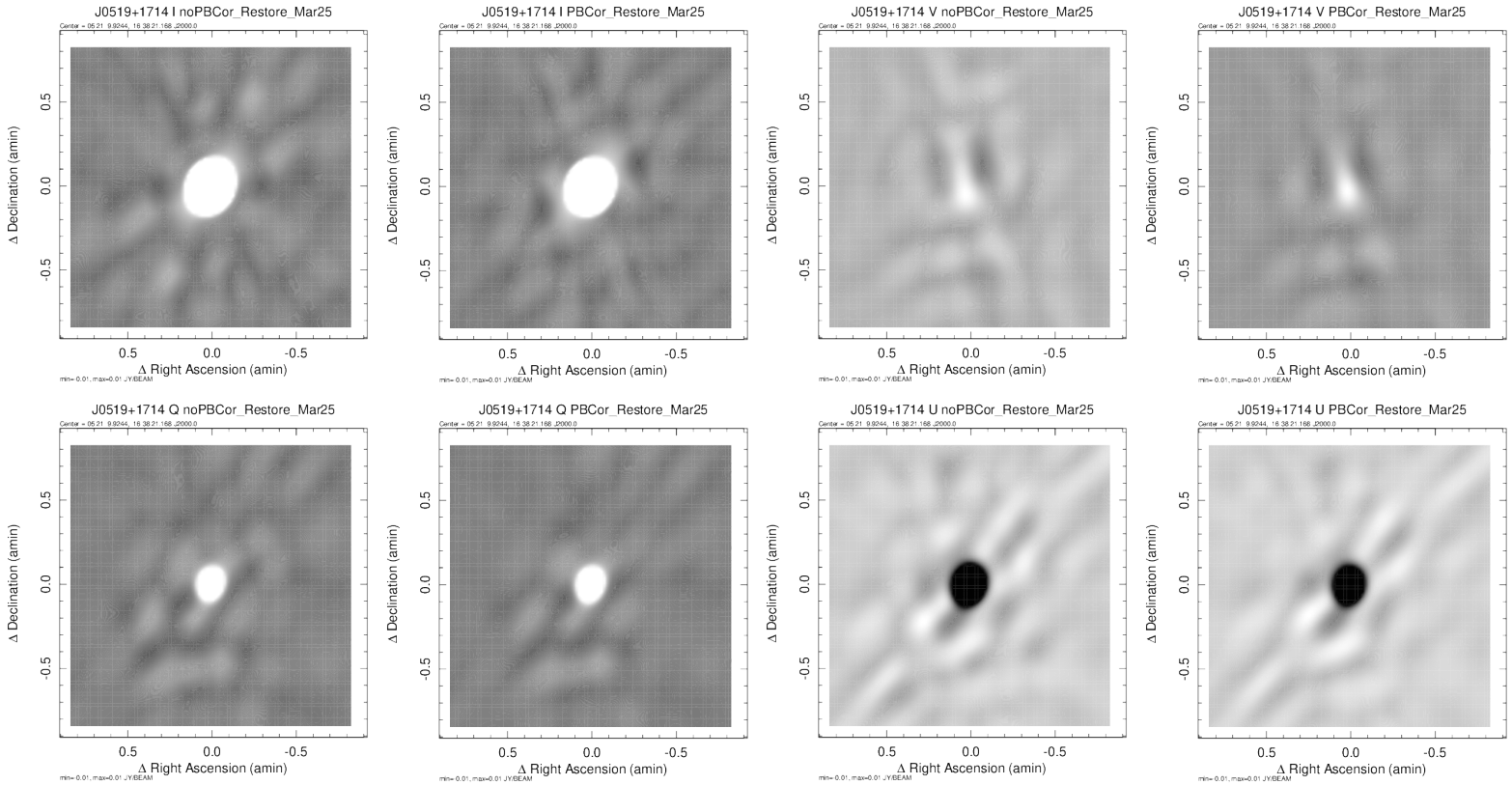

Fig. 28. Like Figure 26 but for J0519+1714.

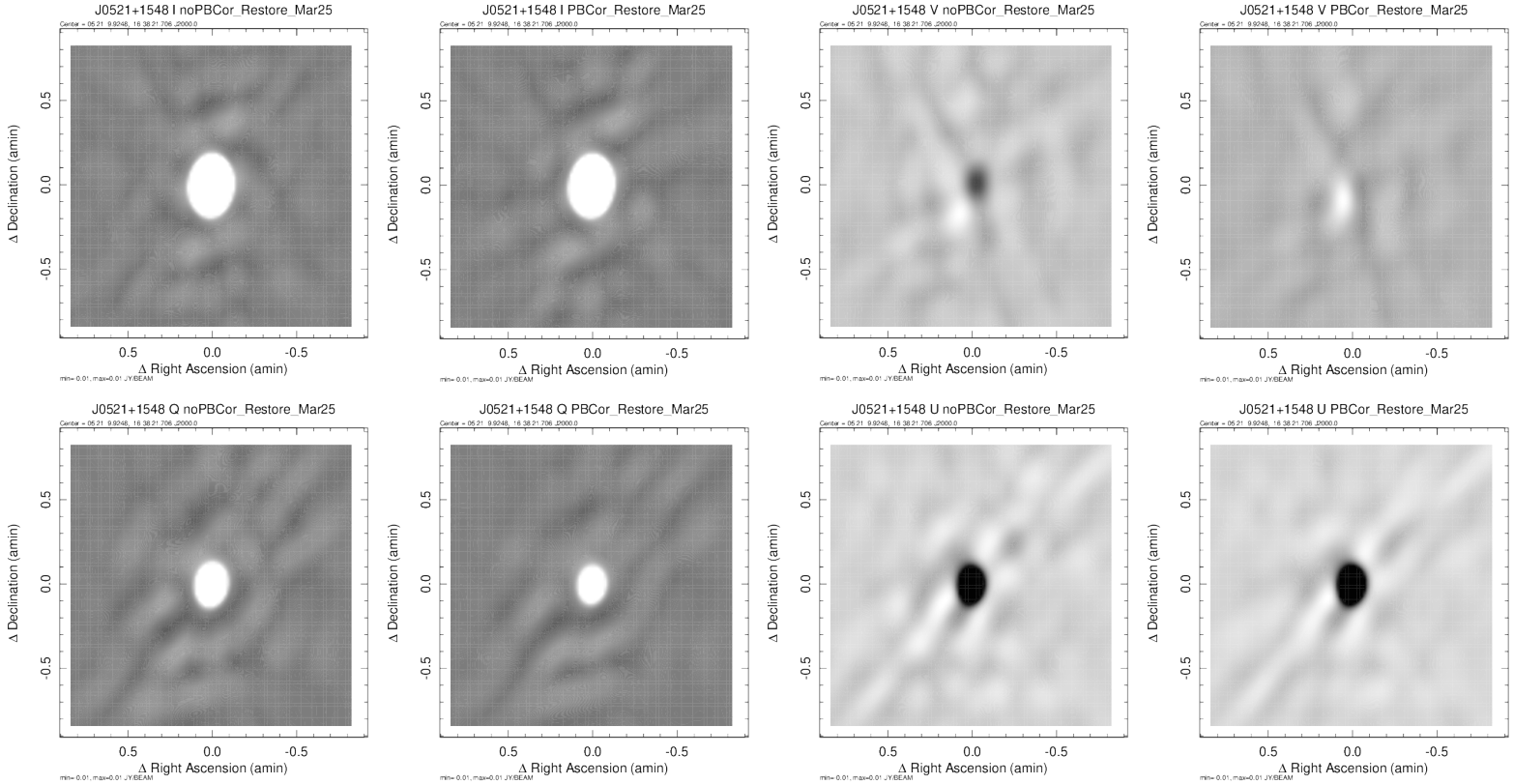

Fig. 29. Like Figure 26 but for J0521+1548

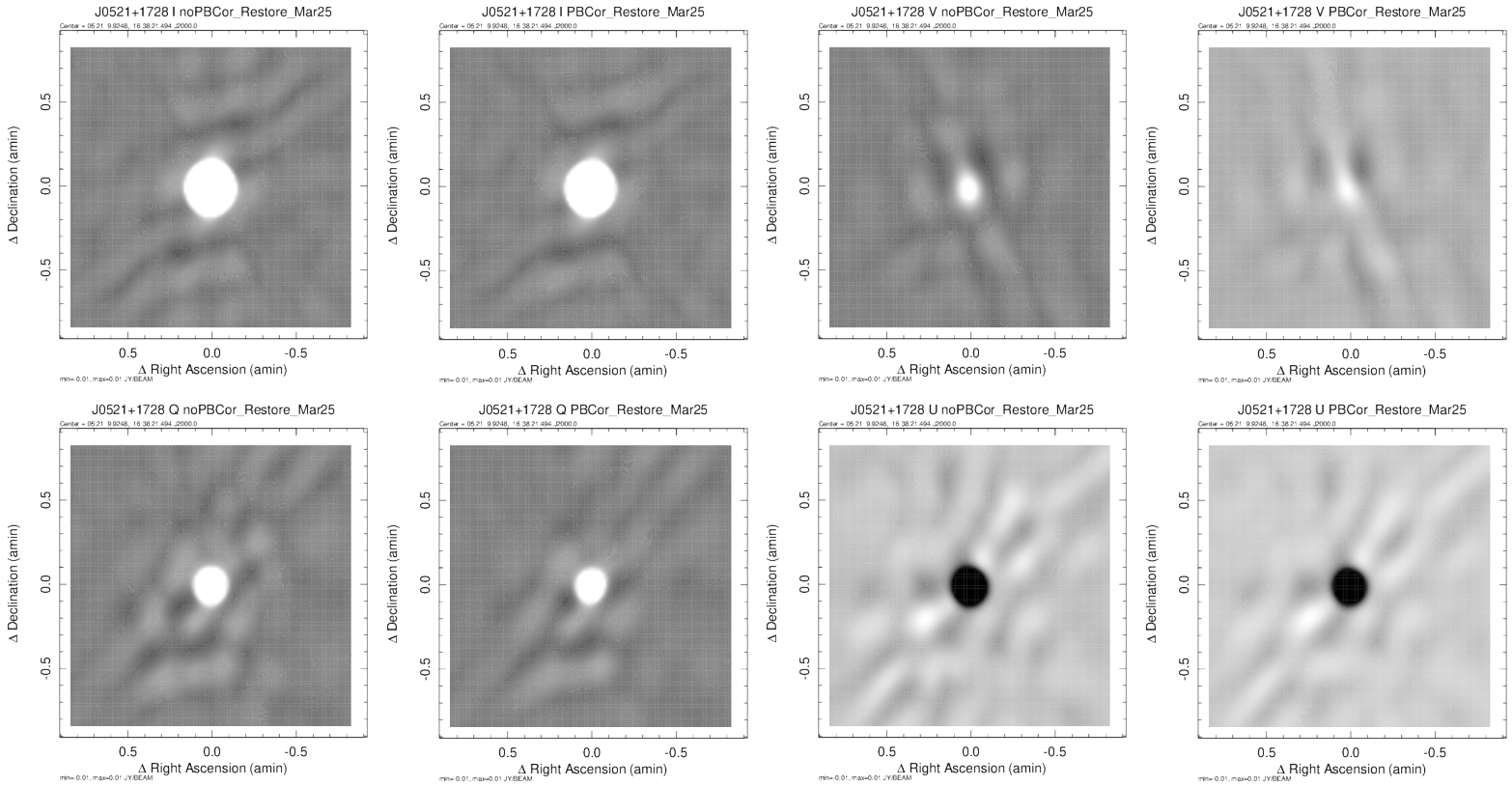

Fig. 30. Like Figure 26 but for J0521+1728.

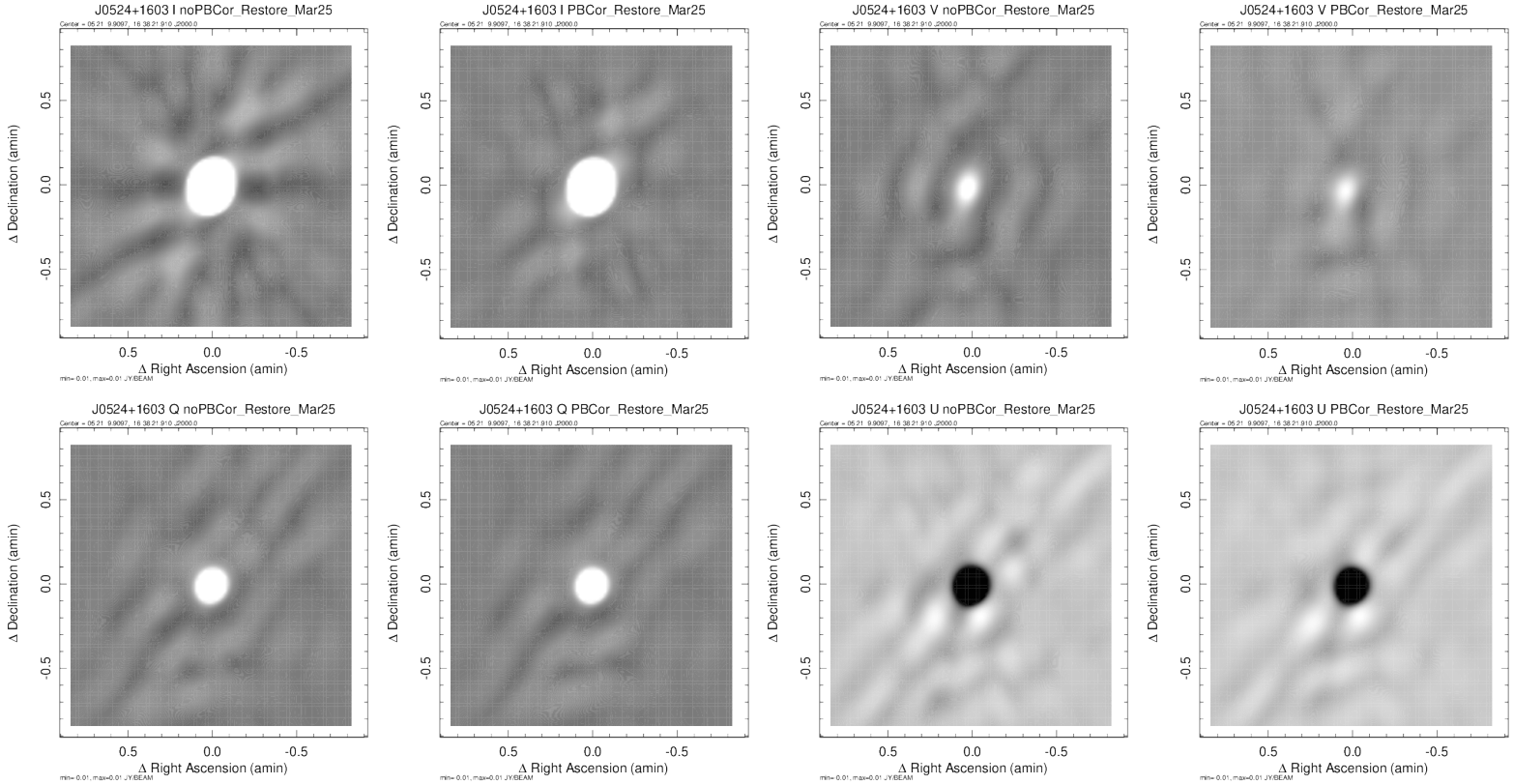

Fig. 31. Like Figure 26 but for J0524+1603.

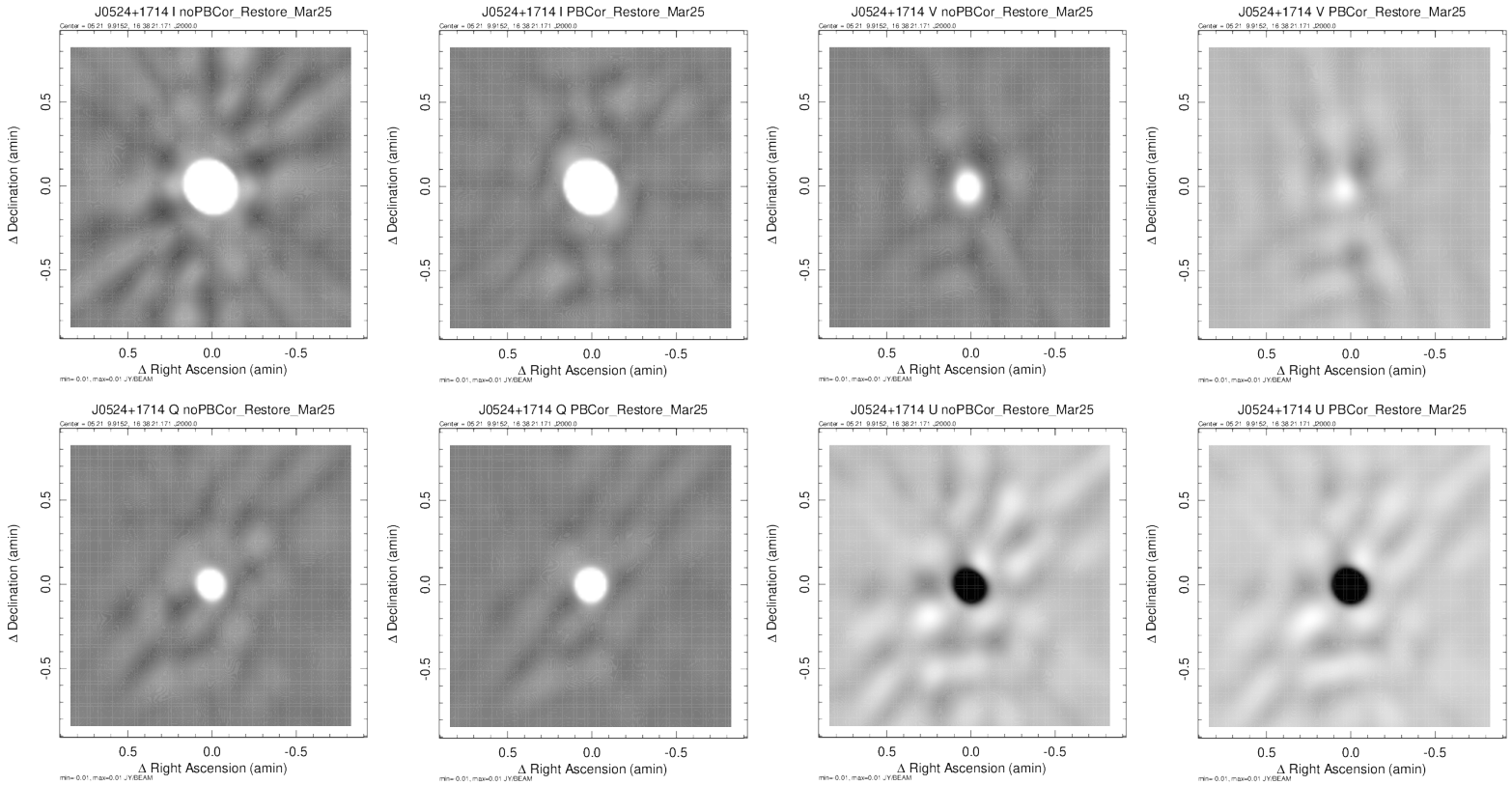

Fig. 32. Like Figure 26 but for J0524+1714.

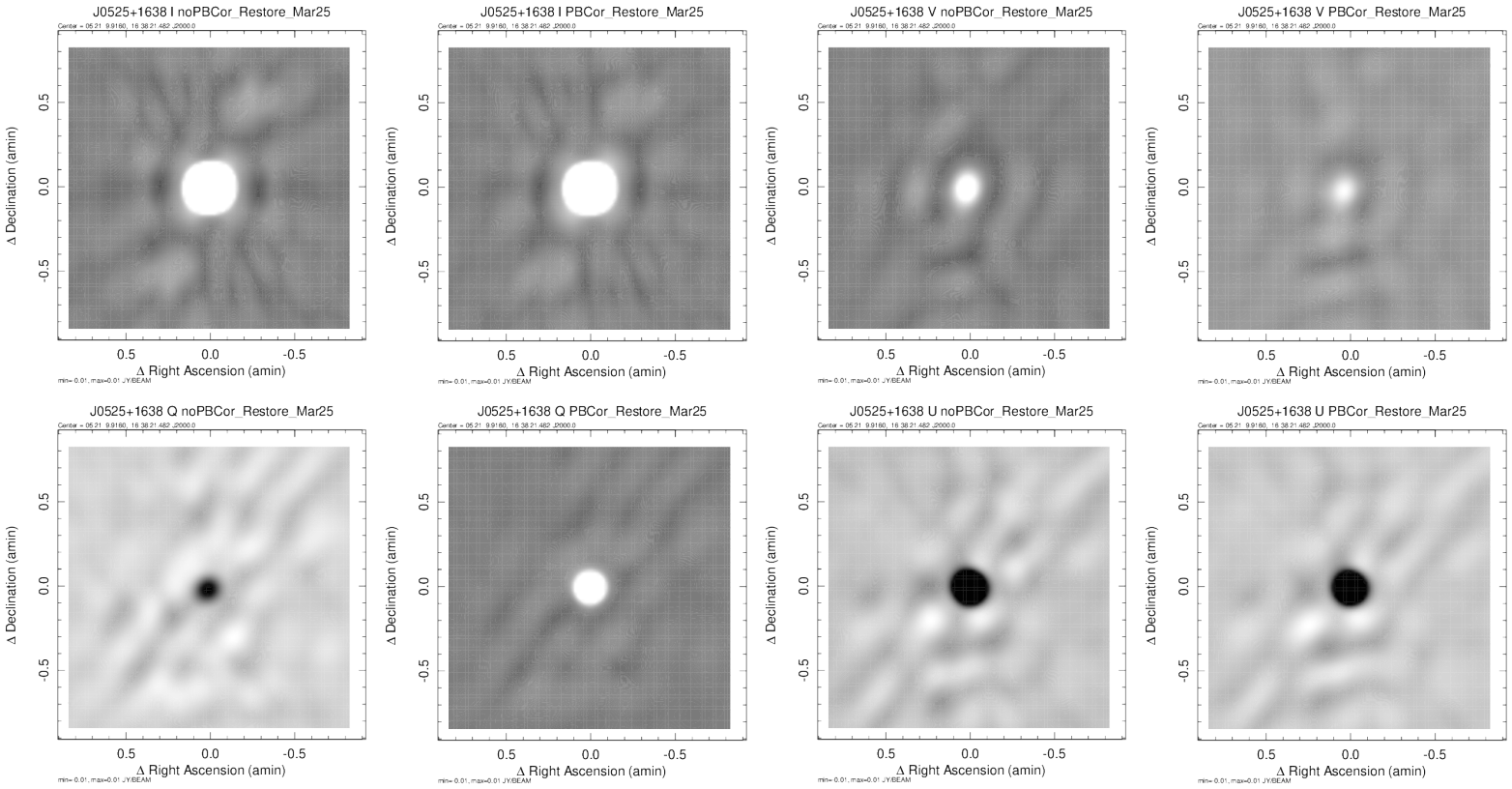

Fig. 33. Like Figure 26 but for J0525+1638.

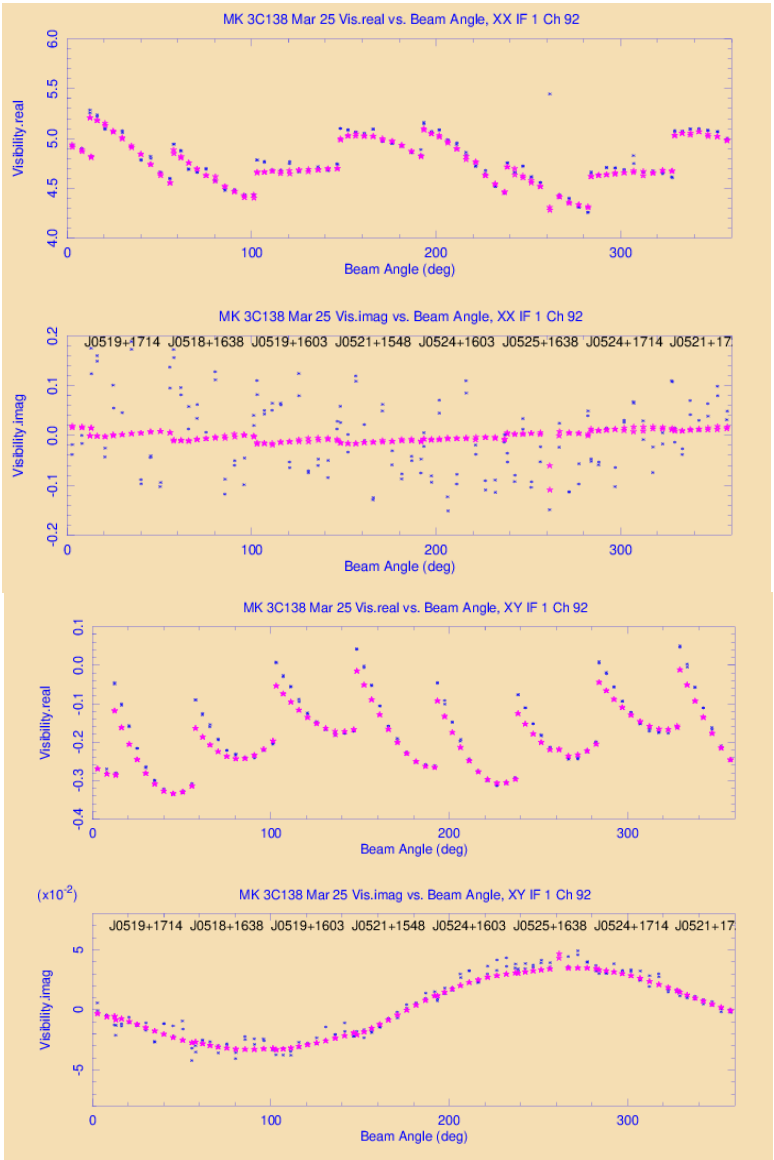

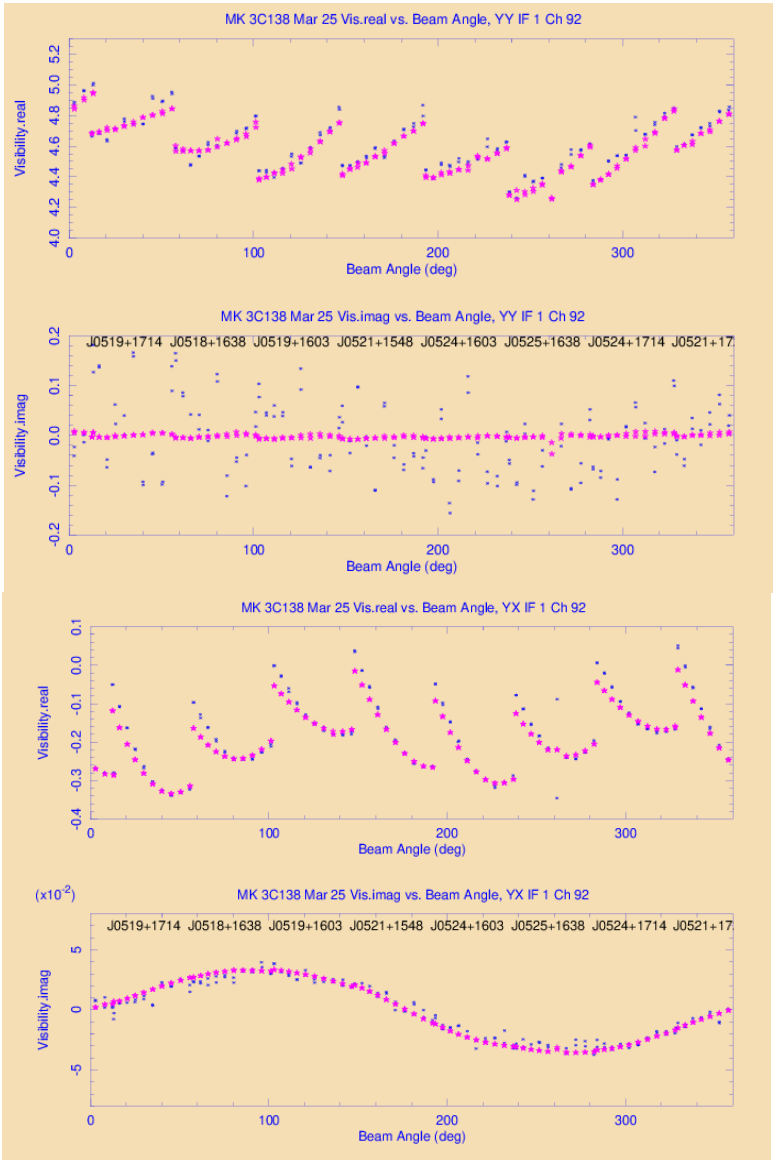

Fig. 34. Like Figure 2 but 3C138 reference pointed offset data from 03 March 2025 on baselines amoung MeerKAT antennas. The data are from channel 92 (of 238) in the first suband(IF), ν=0.924 GHz. Blue *'s are the observed data, the magenta filled stars are model visibilities generated by UVPolCor using a CLEAN model generated by MFBeam including I, Q and U. The pointing names are shown on the imaginary plots centered on the the mean beam angle of the observations for that offset pointing.

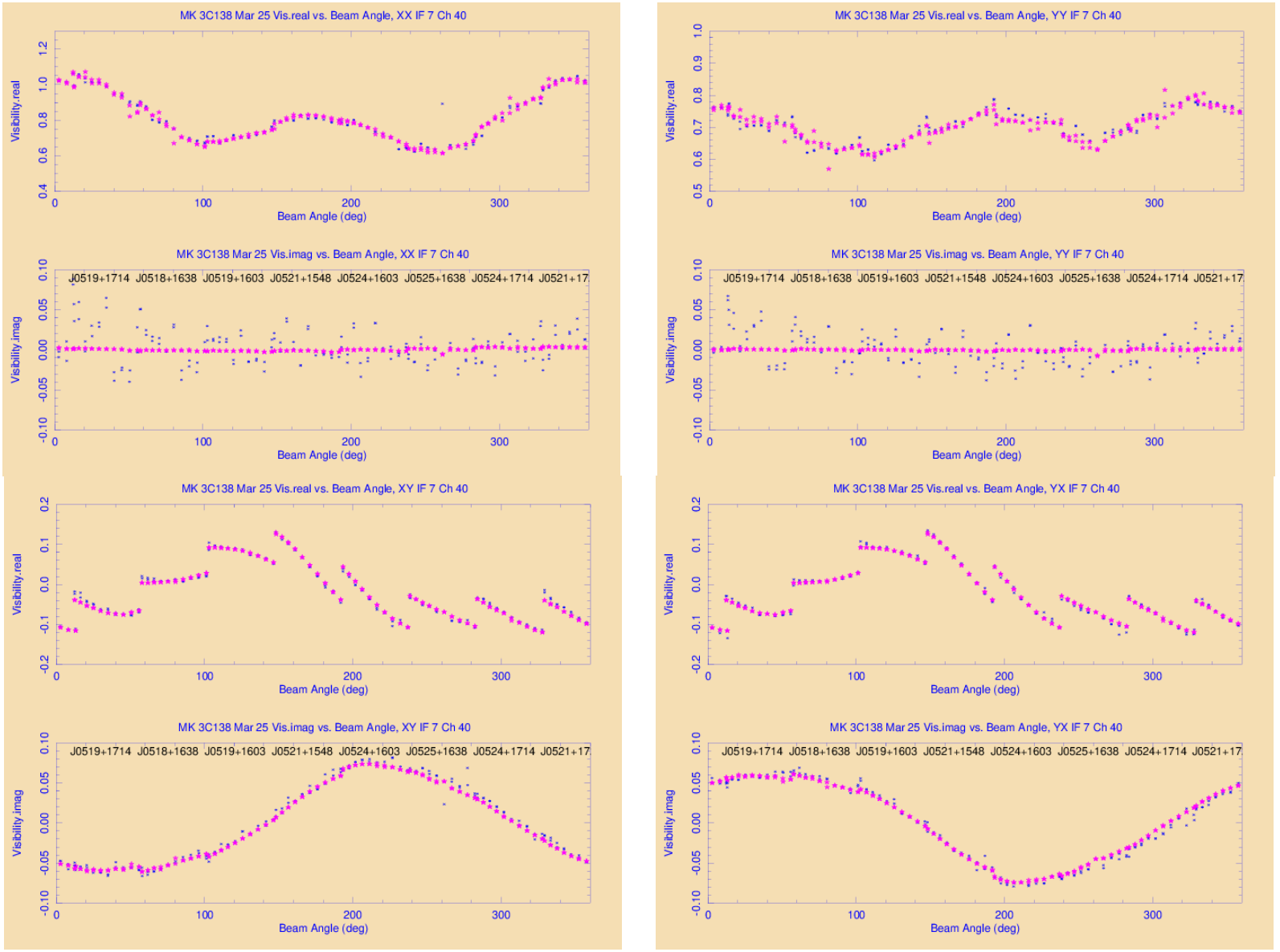

Fig. 35. Like Figure 34 but the data are from channel 40 (of 238) in the seventh of eight suband, ν=1.499 GHz.

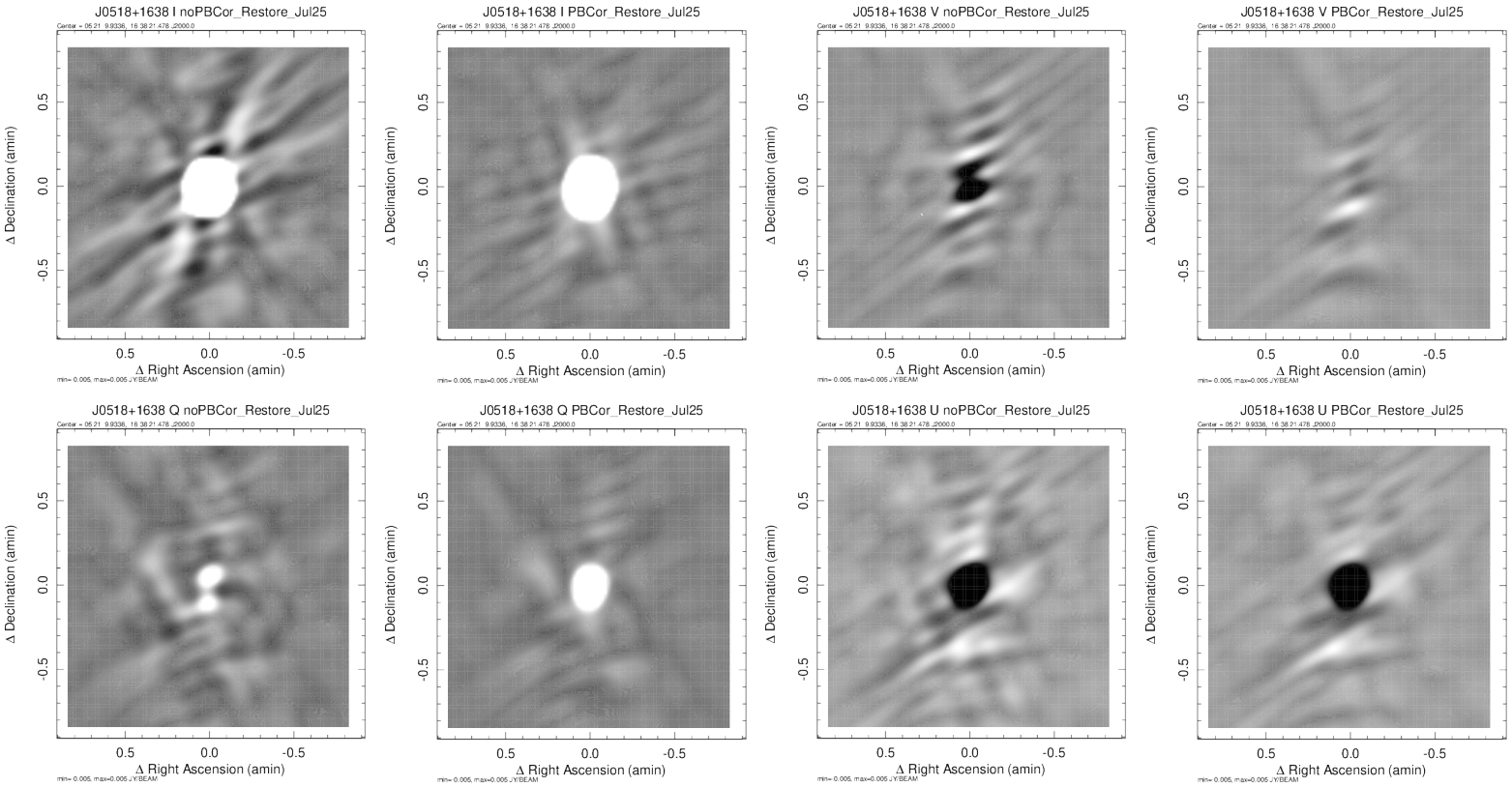

Fig. 36. J0518+1638 Broadband images from MeerKAT + MeerKAT Extension offset pointings of 3C138 from 25 July 2025 as pairs without (left) and with (right) beam corrections. CLEAN was restricted to a single 5 pixel radius circular box centered on the source position and boxes on two nearby sources. to the image. Top row Stokes I (left) and V (right), bottom row Q (left) and U (right). The pixel range displayed is ± 5 mJy/beam.

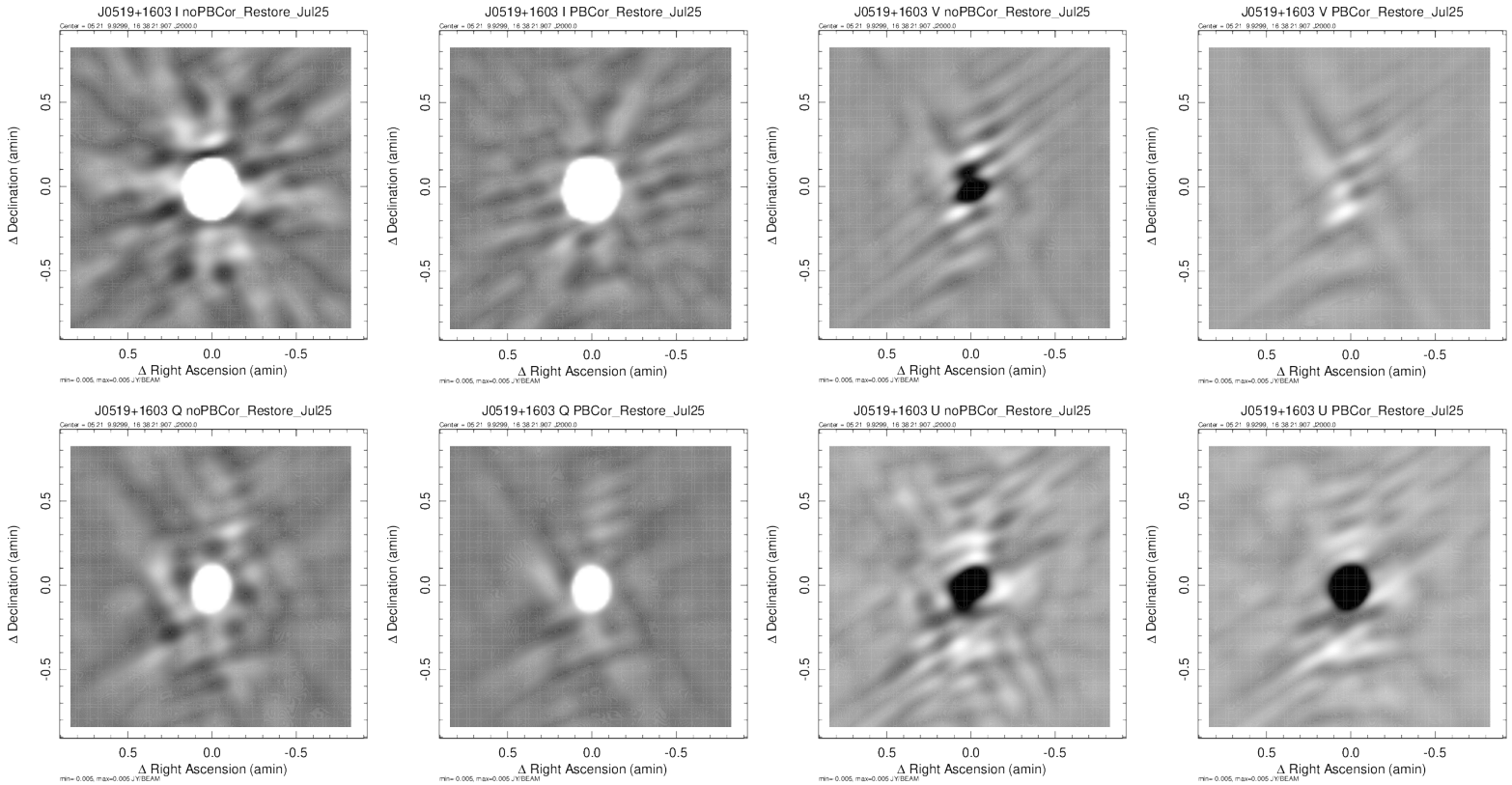

Fig. 37. Like Figure 36 but for J0519+1603.

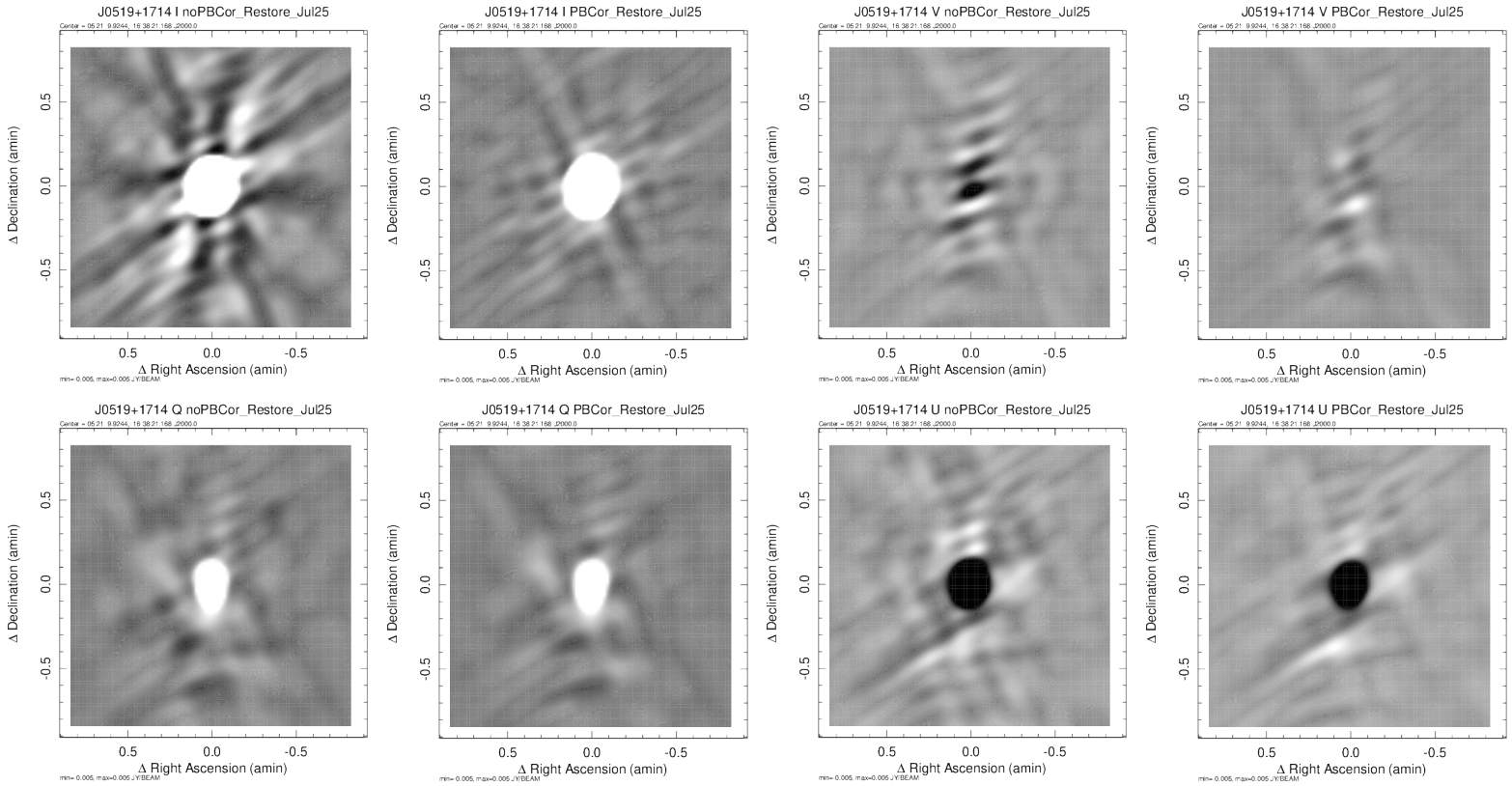

Fig. 38. Like Figure 36 but for J0519+1714.

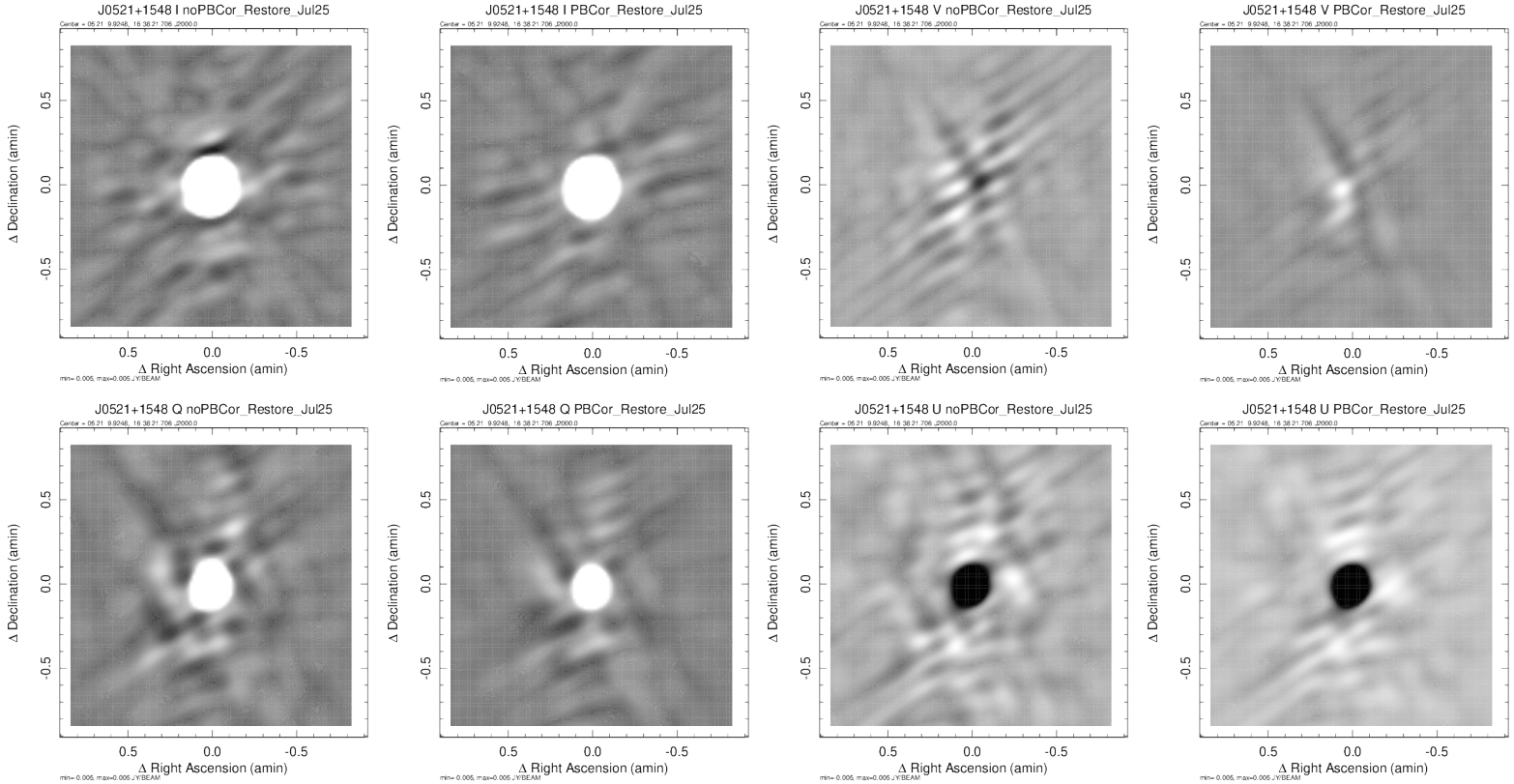

Fig. 39. Like Figure 36 but for J0521+1548

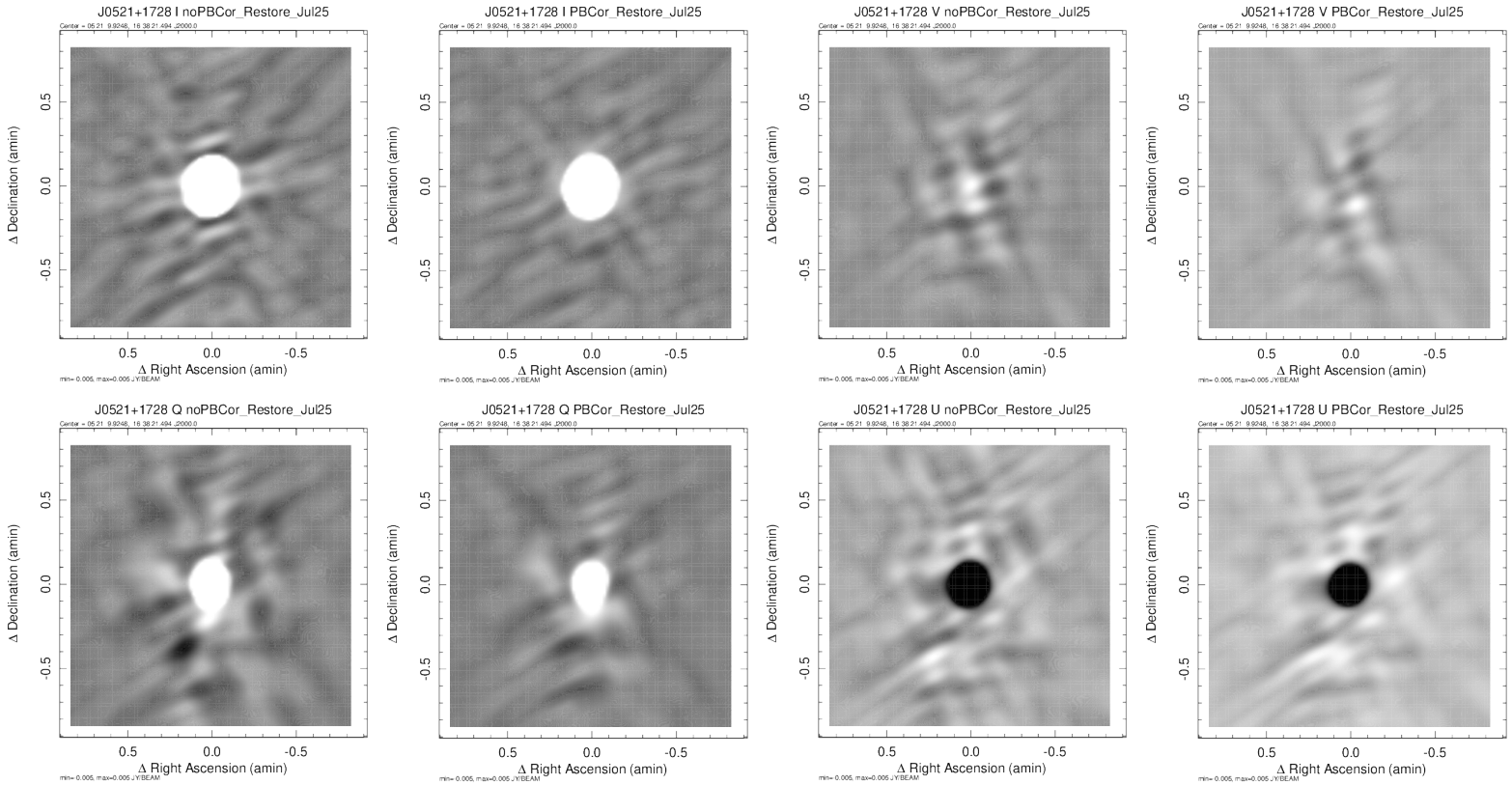

Fig. 40. Like Figure 36 but for J0521+1728.

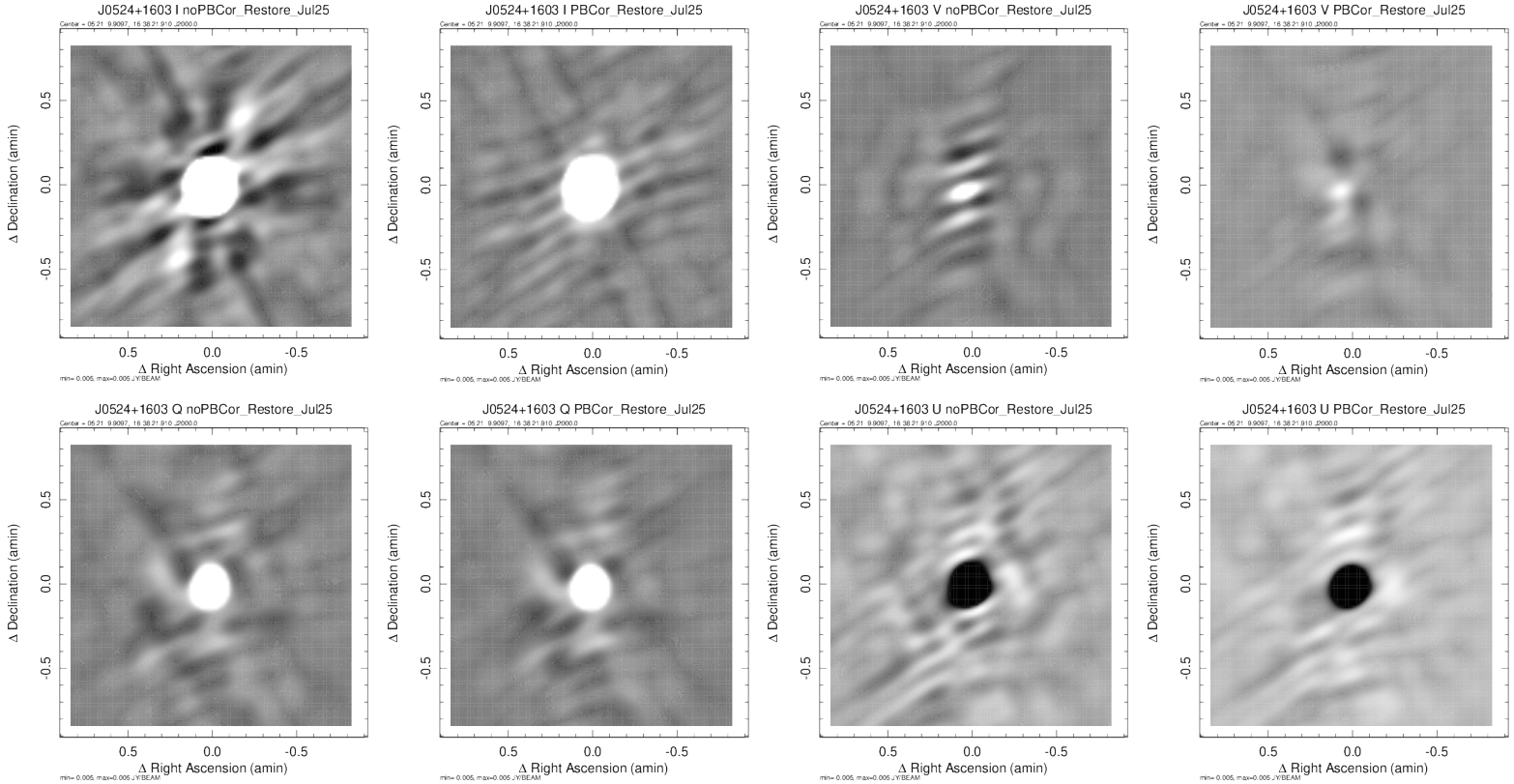

Fig. 41. Like Figure 36 but for J0524+1603.

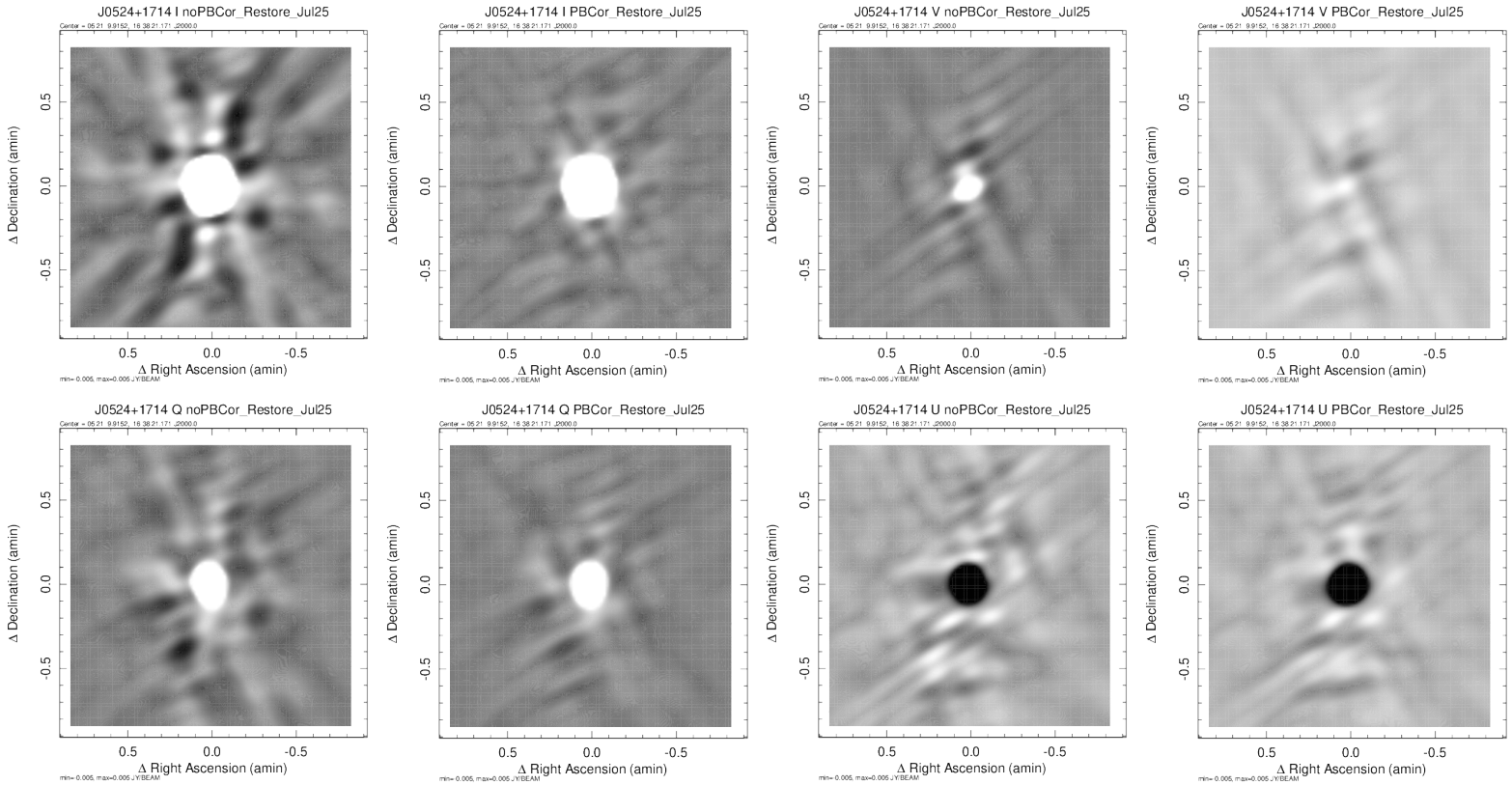

Fig. 42. Like Figure 36 but for J0524+1714.

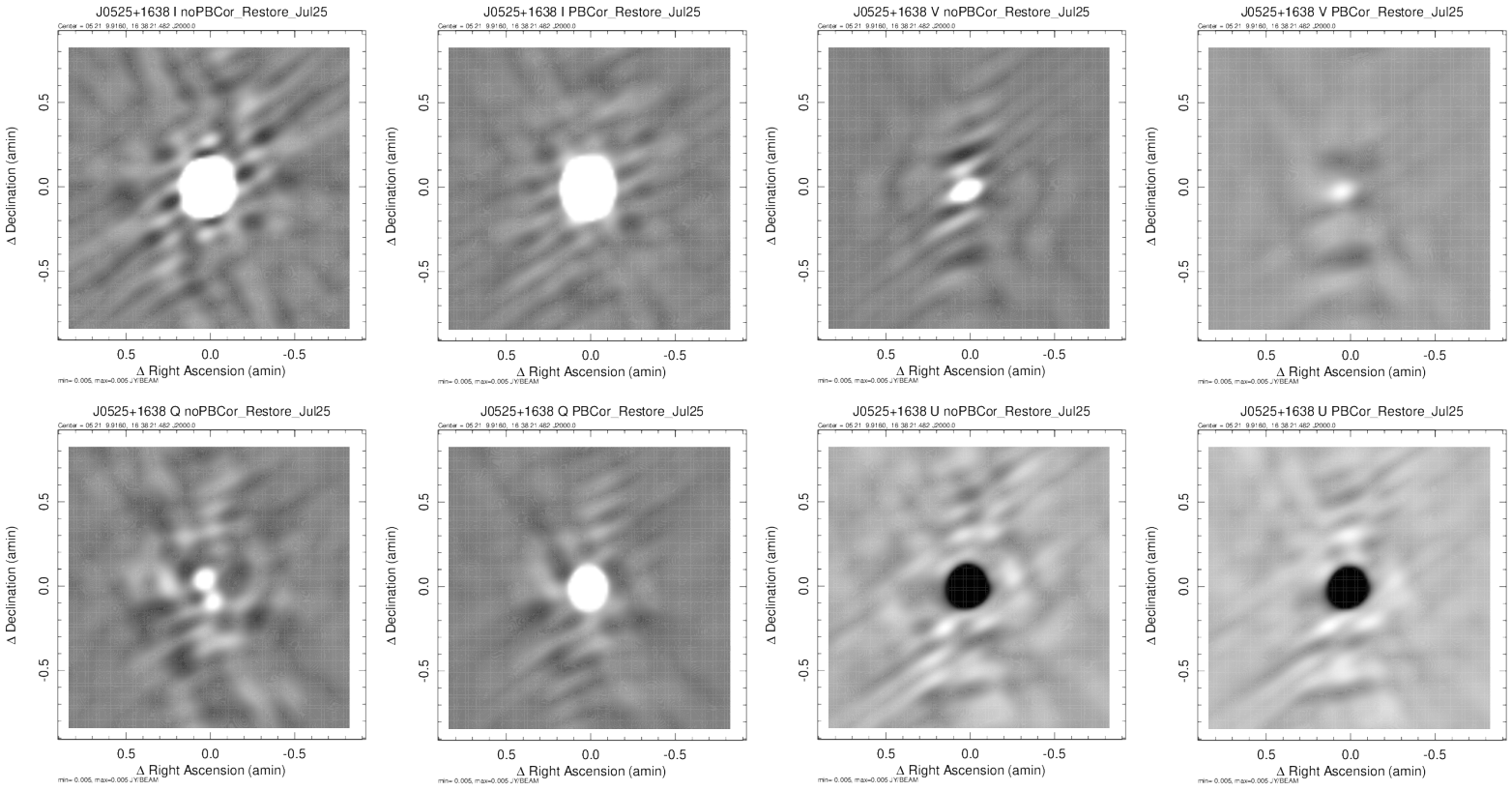

Fig. 43. Like Figure 36 but for J0525+1638.

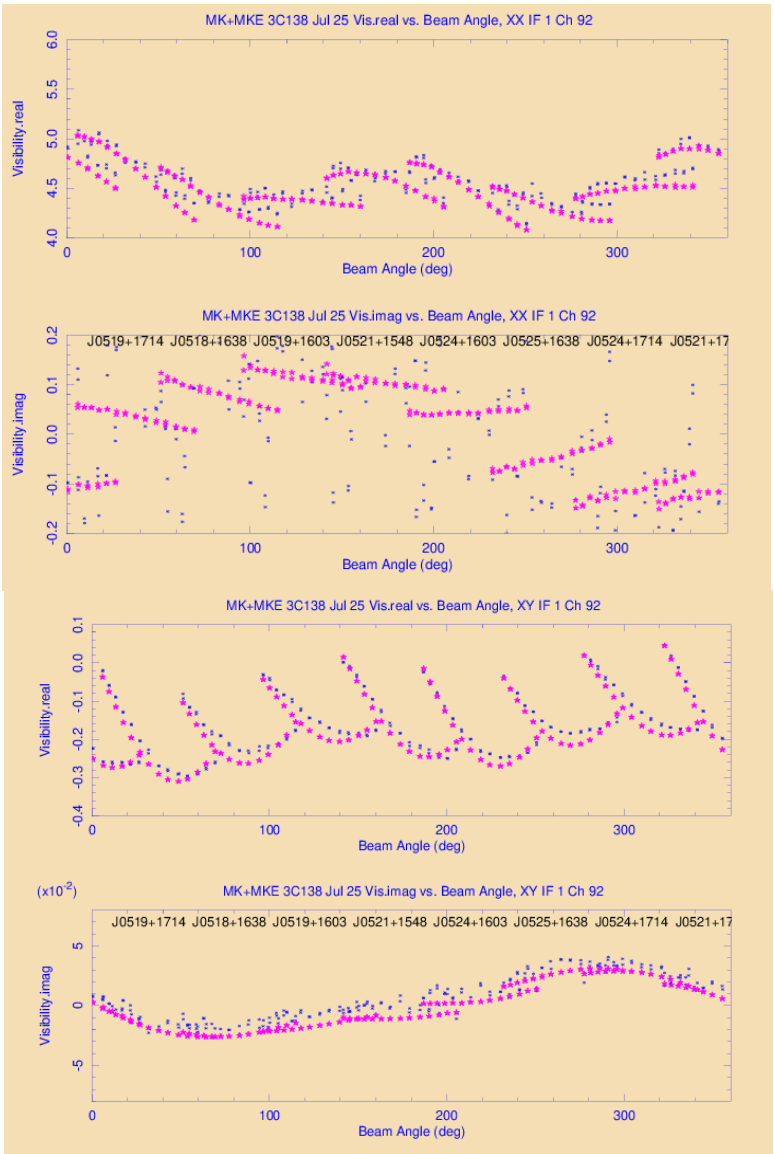

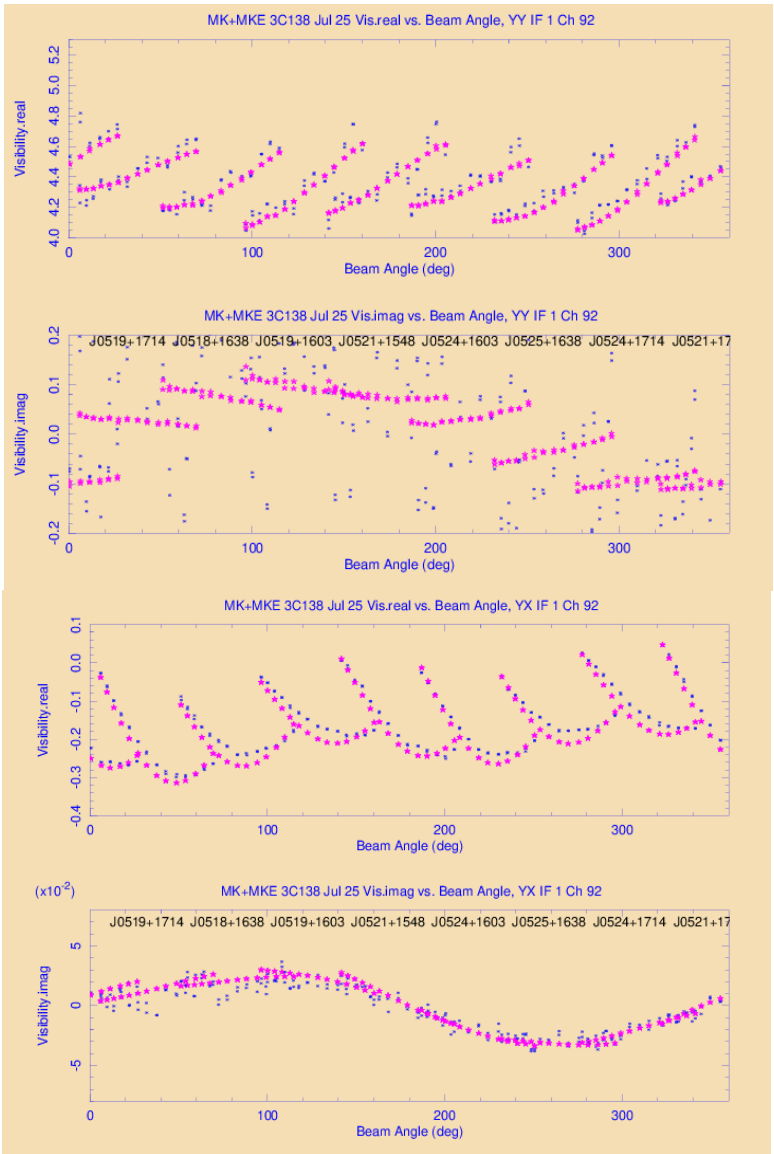

Fig. 44. Like Figure 34 but 3C138 reference pointed offset data from 25 July 2025 on baselines amoung MeerKAT and the MeerKAT Extension antennas. The data are from channel 92 (of 238) in the first suband(IF), ν=0.924 GHz. Blue *'s are the averaged observed data, the magenta filled stars are model visibilities generated by UVPolCor using a CLEAN model generated by MFBeam including I, Q and U. The pointing names are shown on the imaginary plots centered on the the mean beam angle of the observations for that offset pointing.

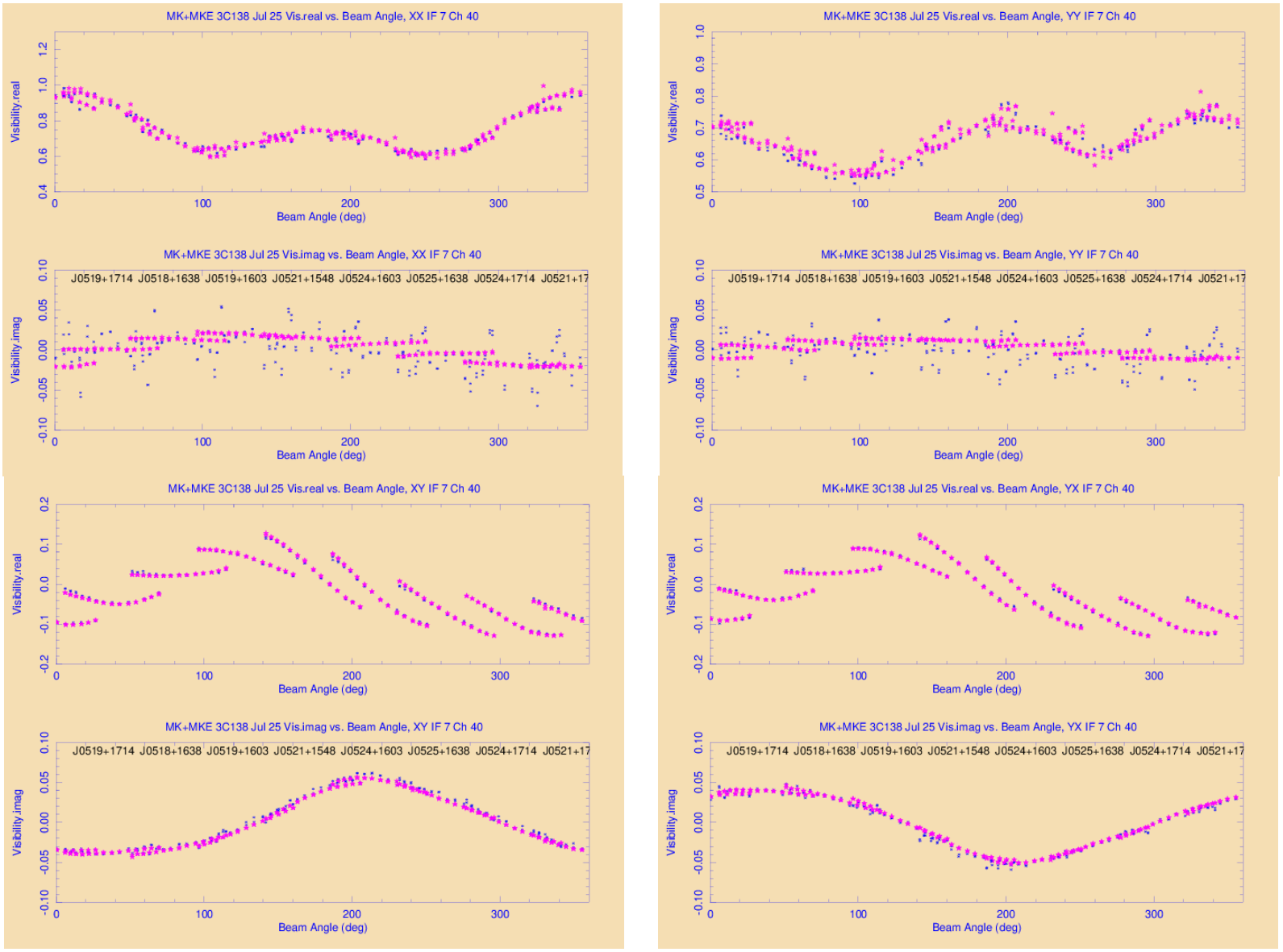

Fig. 45. Like Figure 44 but the data are from channel 40 (of 238) in the seventh of eight subands, ν=1.499 GHz.